An investigation into using ionic liquids for rare earth mineral flotation

Ronghao Li

Department of Mining and Materials Engineering

McGill University

Montreal, Canada

August 2018

A thesis submitted to McGill University in partial fulfillment of the requirements of the degree of Master of Engineering

Acknowledgement

I would like to thank Prof. Waters for giving me the opportunity to accomplish this work. Special thanks to Ray, Chris, Eileen, Gilberto, and Ravi for their help, as well as the rest of min-pro group members for their support through the entire project.

I would like to acknowledge the following persons for their assistance in conducting some of the experiments: Eileen, for her assistance on using XRD, as well as useful advices for FTIR sample preparation and result analysis. Chris, who showed me how to conduct and design an experiment and analyze results, has established a great example of graduate student at McGill University. Ravi and Pengbo, who generously allowed me to take part in their projects, have broaden my horizon in the mineral processing field. Also, I would like to thank Ms. Shiva Naseri and her supervisor Prof. Nazhat from the department of Mining and Materials Engineering at McGill for helping me with FTIR experiment, Mr. Sean Lavoie for his assistance in synthesizing reagents, Dr. Robin Stein from the department of Chemistry at McGill for conducting NMR tests and analyzing results.

In addition, I would like to thank Ms. Barbara Hanley for her help and support through my journey as a master's student. I also want to acknowledge Monique Riendeau and Aleksandra Djuric from the same department at McGill for their assistance and support.

This research is sponsored by an NSERC Discovery grant and the Faculty of Engineering at McGill University.

Last but not the least, I would like to thank my family for their all-time support.

Abstract

Rare earth elements (REE) have been utilized in many cutting-edge applications. Bastnäsite, a flurocarbonate rare earth mineral (REM), is one of the primary sources in REE production. Froth flotation is one of the most commonly applied techniques in REM processing, as well as for the mineral processing industry in general. A type of ionic liquid (IL), tetraethylammonium mono-(2-ethylhexyl)2-ethylhexyl phosphonate ([N_{2222}][EHEHP]), has been investigated previously for REE solvent extraction, and was proven selective and effective. In this work, [N_{2222}][EHEHP] has been investigated as a collector for REM flotation for the first time, with the results compared to quartz and hematite (two gangue minerals commonly associated with REM deposits). Zeta potential measurements and Fourier transfer infrared spectroscopy (FTIR) were used to investigate the surface chemistry of the minerals, the results of which were used to explain microflotation responses. Microflotation results suggest higher collecting ability of IL for quartz and hematite than for bastnäsite, which only showed appreciable recovery at pH 5 with 500 g/t IL. FTIR and zeta potential results suggest adsorption of the phosphonate group onto bastnäsite and hematite, likely through chemisorption; whereas for quartz, the high flotation recovery is likely due to weakly bonded ammonium moiety. To improve the separation efficiency, three depressants, sodium silicate, NorligH (a commercial depressant contains calcium lignin sulfonate), and manganese chloride were tested. Microflotation tests show that the tested depressants can significantly depress bastnäsite at all tested conditions, with limited impact on hematite and quartz. A synthetic mixture of three minerals was tested in bench scale flotation at pH 5 with sodium silicate. Results show that bastnäsite was selectively depressed, with the recovery of hematite and quartz remaining almost unchanged. A better separation could be achieved following such reverse flotation route, possibly with a higher collector dose and a more effective depressant. A pretreatment stage is suggested to reject some of the gangue minerals before flotation in order to improve separation efficiency.

Résumé

Les éléments des terres rares (ETR) sont utilisés dans de nombreuses domaines innovatives. Le Bastnaésite, un minéral des terres rares (MTR) fluorocarboné, est l'une des sources principales de production des ETR. La flottation par mousse est l'une des techniques les plus communément utilisées dans le traitement des MTR ainsi que dans l'industrie minéralurgique en général. Une liquide ionique (LI), le tetraethylammonium mono-(2-ethylhexyl)2-ethylhexyl phosphonate ($[N_{2222}][EHEHP]$), a été étudiée auparavant pour l'extraction par solvant des ETR et s'est démontrée comme étant sélectif et efficace. Ce projet étudie l'utilisation du $[N_{2222}][EHEHP]$ comme collecteur pour la flottation des MTR. Les résultats sont comparés au quartz et à l'hématite (deux minéraux de la gangue couramment associés aux dépôts MTR). Des mesures du potentiel zêta et la spectroscopie infrarouge à transformée de Fourier (IRTF) ont été utilisées pour étudier la chimie de surface des minéraux. Ces résultats ont été utilisés pour supporter des données de microflottation obtenus auparavant. Les résultats de microflottation suggèrent que la capacité de collecte du LI est plus élevée pour le quartz et l'hématite que pour le bastnaésite, qui n'a montré qu'une récupération appréciable à un pH de 5 avec 500 g/t de LI. Les résultats du potentiel zêta et de l'IRTF suggèrent une adsorption du groupe phosphonate sur le bastnaésite et l'hématite, probablement par le mécanisme de chimisorption, tandis que pour le quartz, la récupération élevée de la flottation est possiblement due au groupe de l'ammonium faiblement lié. Pour prouver l'efficacité de la séparation, trois dépresseurs ont été testés, soit le silicate de sodium, le NorligH (un dépresseur commercial contenant du lignine sulfonate de calcium) et le chlorure de manganèse. Les résultats des tests de microflottation montrent que les dépresseurs peuvent réduire considérablement le bastnaésite dans toutes les conditions testées, avec peu d'impact sur l'hématite et le quartz. Un mélange synthétique de trois minéraux a été testé par flottation en laboratoire à un pH de 5 avec le silicate de sodium. Les résultats montrent que le bastnaésite a été sélectivement diminué tandis que la récupération de l'hématite et du quartz est restée considérablement stable. Une meilleure séparation pourrait être obtenue en utilisant la méthode de la flottation inverse avec une dose de collecteur plus élevée et un dépresseur plus efficace. Une étape de prétraitement est proposée pour rejeter certains minéraux de la gangue avant la flottation afin d'améliorer l'efficacité de la séparation.

Table of Contents

Table of Figures

Table of Tables

Chapter 1. Introduction

The rare earth elements (REE) include 15 lanthanides and yttrium, which have similar chemical properties (Gupta, et al., 1992; Jordens, et al., 2014). They can be further classified as light rare earth elements (LREE) including La to Eu, and heavy rare earth elements (HREE) including Gd to Lu and Y (Gupta, et al., 1992). Unlike other elements on the periodic table, the ionic radius of the lanthanides reduces as atomic number increases (Krishnamurthy, et al., 2005). This phenomenon is named the "lanthanide contraction", and can be explained by the increasing charge on the nucleus pulling the electron shells closer (Spedding, 1975). Despite what their name implies, REE are moderately abundant elements in the earth crust, such that their total abundance is approximately 240 ppm, higher than elements including carbon, lead, silver, and mercury (Krishnamurthy, et al., 2005; Jordens, et al., 2013). Nevertheless, the availability of individual REE are highly unequal that their relative abundance vary from 0.52 ppm for thulium to 66 ppm for cerium (Krishnamurthy, et al., 2005). In general, REE with an even atomic number are more abundant than those with odd atomic number (Kilbourn, 1988); those with lower atomic number are more concentrated than others because the larger radii make the atoms more incompatible with other atoms (Krishnamurthy, et al., 2005).

REE receive their names because deposits with commercially high concentration are rare, and it is difficult to separate individual REE from each other due to their similar properties (Fernandez, 2017; Krishnamurthy, et al., 2005). Even though REE are relatively abundant in the earth crust, rare earth mineral (REM) deposits, however, are not evenly distributed across the world. In addition, REM deposits with minable and economic concentrations are less common than other ores (U.S. Geological Survey, 2018; Krishnamurthy, et al., 2005). The total reserve of rare earth oxides (REO) are estimated as 100 million tons distributed in over 30 countries (Chen, 2011). The main RE producers with their mine production in the past years and reserves are compared in Table 1.1.

REE have been utilized in many high-technology applications such as magnets, catalysts, hydrogen storage, electronic devices, ceramics, and polishing powders (Argus Consulting Services, 2015; Krishnamurthy, et al., 2005). The global demand for REE in 2010 and the predicted values for 2020 are displayed in Table 1.2. From Table 1.2, it can be observed the total

demand will double by 2020; higher demand growth is expected for catalysts, magnets, and phosphors than other applications.

Table 1.1. RE mine production and reserve in the world, data adapted from (U.S. Geological Survey, 2018).

Country	Mine Production (Thousand tons)		Reserves (Thousand tons)
	2016	2017	
Australia	15	20	3400
Brazil	2.2	2	22000
Canada	-	-	830
China	105	105	44000
Greenland	-	-	1500
India	1.5	1.5	6900
Malawi	-	-	140
Malaysia	0.3	0.3	30
Russia	2.8	3	18000
South Africa	-	-	860
Thailand	1.6	1.6	NA
United States	-	-	1400
Vietnam	0.22	0.1	22000
Total	129	130	120000

Table 1.2. Global demand for REE, data adapted from (Krishnamurthy, et al., 2005).

Applications	2010		2020	
	Tons	% of total demand	Tons	% of total demand
Alloys	22000	17.6%	32100	12.2%
Catalysts	245	0.2%	51500	19.5%
Ceramics	7000	5.6%	13800	5.2%
Glass	11000	8.8%	14850	5.6%
Magnets	26000	20.8%	88600	33.6%
Phosphors	8500	6.8%	20200	7.7%
Polishes	19000	15.2%	31050	11.8%
Others	7000	5.6%	11450	4.3%
Total	125000	100.0%	263550	100.0%

Chapter 2. Literature Review

2.1 Rare earth minerals (REM) and common gangue

Currently, more than 250 REM have been discovered; they commonly exist in the forms of carbonates, oxides, phosphates, and silicates (Gupta, et al., 1992; Krishnamurthy, et al., 2005). REM appear primarily in four geologic environments: carbonatites, alkaline igneous systems, ion-adsorption clay deposits, and monazite-xenotime-bearing placer deposits (U.S. Geological Survey, 2018). Historically, the bulk of REE supply comes from bastnäsite (a carbonate mineral, (Ce, La, Y)FCO_3), heavy beach sand, and ion-adsorbed clays (Jordens, et al., 2013). Among all RE resources, carbonatites and placer deposits are the primary production sources of LREE; ion-adsorption clays are the primary production source of HREE (U.S. Geological Survey, 2018). Currently, approximately 95% of the world's RE resources are extracted from three minerals: bastnäsite, monazite ((Ce, La, Th, Y)PO_4), and xenotime (YPO_4) (Long, et al., 2010; Gupta, et al., 1992).

Monazite is a phosphate REM, which contains approximately 70% REO (Krishnamurthy, et al., 2005). The elements occupying its REE sites in the lattice are interchangeable, and therefore the elemental composition might differ depending on the deposit. Monazite in general contains 20-30% Ce_2O_3, 10-40% La_2O_3, ~5% Y_2O_3, 4-12% Th, and significant amounts of Nd, Pr, and Sm (Krishnamurthy, et al., 2005). The most important source of monazite is beach placers, which also contain other minerals including ilmenite, rutile, and zircon (Krishnamurthy, et al., 2005). Monazite has been found in large quantities in Australia, Brazil, China, India, Malaysia, South Africa, and USA; it has been extracted from deposits include Van Rhynsdorp and Naboomspruit (South Africa), Colorado (USA) and Bayan Obo (China) (Krishnamurthy, et al., 2005). Xenotime is another phosphate mineral mainly bearing yttrium; it contains about 67% REO, most of which are heavies (Krishnamurthy, et al., 2005). Xenotime usually co-exists with monazite in placer deposits, with a much lower content than monazite (about 0.5-5% of the content of monazite) (Krishnamurthy, et al., 2005).

Bastnäsite is a flurocarbonate mineral which contains about 70% REO; most of its RE content are LREE (Krishnamurthy, et al., 2005). Bastnäsite is the primary source of light rare earth oxides (LREO) in the Bayan Obo deposit in China and Mountain Pass in USA, two of the biggest RE

deposits in the world (Krishnamurthy, et al., 2005). Similar to monazite and other REM, the composition of bastnäsite may be different depending on the mineral origin. For instance, REE distribution in bastnäsite of Bayan Obo and Mountain Pass deposits are shown in Table 2.1. The elemental composition of bastnäsite are not exactly the same in these two deposits. In both deposits, La, Ce, Pr, Nd, and Sm are the main REE in bastnäsite, with some other elements with less amounts (Table 2.1). Due to its importance in REE (especially LREE) production and the abundance in large deposits such as Bayan Obo deposit (China) and Mountain Pass (USA), bastnäsite was chosen for investigation in this work.

Table 2.1. REE distribution in bastnäsite from Mountain Pass and Bayan Obo deposits, data adapted from (Hedrick, 1991).

REE	Mountain Pass, USA	Bayan Obo, China
La	33.2%	23.0%
Ce	49.1%	50.0%
Pr	4.34%	6.20%
Nd	12.0%	18.5%
Sm	0.789%	0.800%
Eu	0.118%	0.200%
Gd	0.166%	0.700%
Tb	0.0159%	0.100%
Dy	0.0312%	0.100%
Y	0.0913%	0.500%
Ho	0.0051%	Trace
Er	0.0035%	Trace
Tm	0.0009%	Trace
Yb	0.0006%	Trace
Lu	0.0001%	Trace

In flotation, dissolved species from a mineral surface can undergo hydrolysis, complexation, adsorption, and precipitation reactions (Somasundaran, et al., 2007). The products of metal ion hydrolysis reactions, including hydroxyl complexes and hydroxide precipitate, could be active at the mineral surface and change surface properties (Wills & Finch, 2016). These species could interact with reagents and affect the adsorption, and therefore influence the flotation response (Somasundaran, et al., 2007). Therefore, it is important to understand the possible ion species near the interface of the particle and surrounding solution. For bastnäsite, the ion species of Ce^{3+} in water have been studied by Pradip et al. (1983). The following hydrolysis reactions (as shown in Eq. (2.1)-(2.4)) of Ce^{3+} and their reaction constants are adapted from previous work (Ren, et al., 1997; Wang, et al., 2014). Based on these equations, an ion speciation diagram was generated as

seen in Figure 2.1 (adapted from (Wang, et al., 2014)). In the acidic pH range (pH<7), Ce^{3+} is the dominant ion species; as pH increases, Ce^{3+} start forming hydroxides such as $Ce(OH)^{2+}$, $Ce(OH)_2^+$, and $Ce(OH)_3$. As pH increases further to 12 and above, $Ce(OH)_4^-$ becomes the predominant species in the system.

$$Ce^{3+} + H_2O \rightleftharpoons Ce(OH)^{2+} + H^+ \qquad K_1 = 10^{5.9} \qquad \text{Eq. (2.1)}$$

$$Ce(OH)^{2+} + H_2O \rightleftharpoons Ce(OH)_2^+ + H^+ \qquad K_2 = 10^{5.8} \qquad \text{Eq. (2.2)}$$

$$Ce(OH)_2^+ + H_2O \rightleftharpoons Ce(OH)_3 + H^+ \qquad K_3 = 10^{4.3} \qquad \text{Eq. (2.3)}$$

$$Ce(OH)_3 + H_2O \rightleftharpoons Ce(OH)_4^- + H^+ \qquad K_4 = 10^{2.0} \qquad \text{Eq. (2.4)}$$

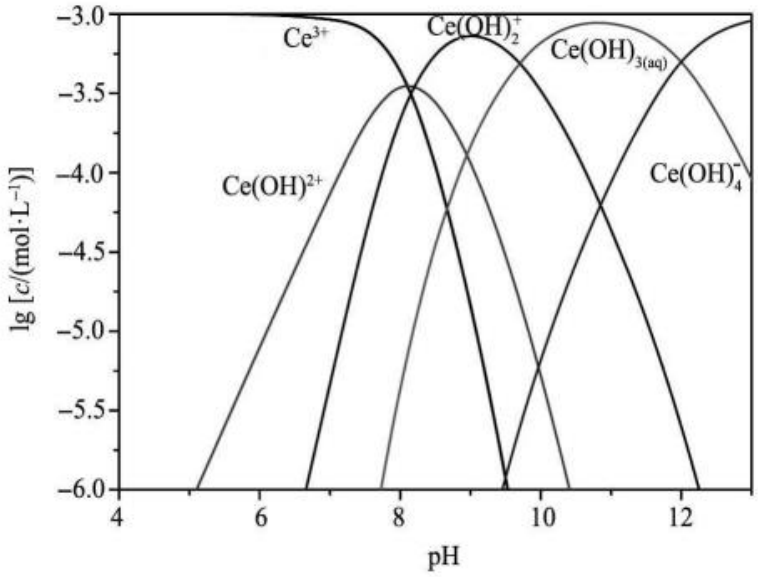

Figure 2.1. Ion speciation diagram of Ce^{3+}, initial Ce^{3+} concentration is 10^{-3} mol/L, figure adapted from (Wang, et al., 2014).

REM deposits, like many other mineral deposits, contain a large amount of low or non-valuable minerals (gangue minerals). For example, the Nechalacho deposit (Canada), which is one of the largest REM deposits outside of China, contains silicate (*e.g.* quartz) and iron oxide minerals (*e.g.* hematite) as gangue (Jordens, et al., 2016). These gangue minerals were chosen for investigation in this project due to their differences in chemical composition, surface properties, and physical properties etc. The following section will briefly review these two minerals.

Hematite (Fe_2O_3) is a gangue mineral that is naturally hydrophilic. In order to understand the response of hematite in flotation process, the hydrolysis reactions of Fe^{3+} ion have been previously

investigated by Fuerstenau et al. (1965). The reactions and the reaction constants were summarized by (Jin, et al., 2016) as following:

$$Fe^{3+} + H_2O \rightleftharpoons FeOH^{2+} + H^+ \qquad K_1 = 6.46 \times 10^{-3} \qquad \text{Eq. (2.5)}$$

$$Fe^{3+} + 2H_2O \rightleftharpoons Fe(OH)_2^+ + 2H^+ \qquad K_2 = 2.00 \times 10^{-6} \qquad \text{Eq. (2.6)}$$

$$Fe^{3+} + 3H_2O \rightleftharpoons Fe(OH)_{3(aq)} + 3H^+ \qquad K_3 = 1.12 \times 10^{-10} \qquad \text{Eq. (2.7)}$$

$$Fe(OH)_{3(s)} + 3H^+ \rightleftharpoons Fe^{3+} + 3H_2O \qquad K_4 = 1.58 \times 10^{3} \qquad \text{Eq. (2.8)}$$

Based on these equations, a speciation diagram of ferric ions (with initial ion concentration 10^{-4} mol/L) was drawn (Figure 2.2). It can be observed that Fe^{3+}, $FeOH^{2+}$ and $Fe(OH)_2^+$ are the dominant ion species at pH<5; at pH 5 or above, $Fe(OH)_3$ is the species that is most likely present on hematite surface.

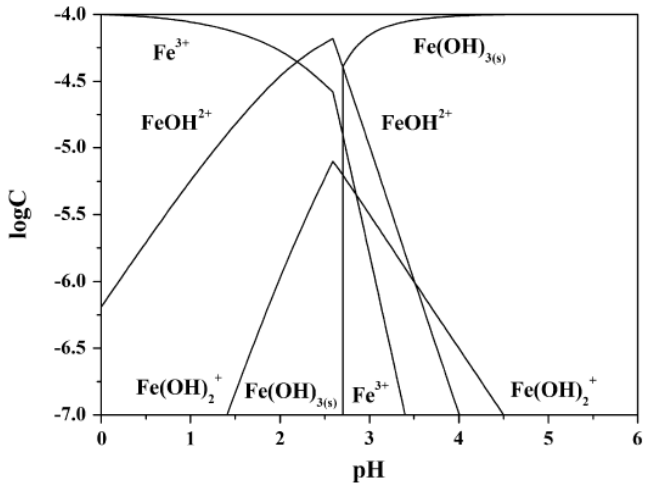

Figure 2.2. Ion speciation diagram of Fe^{3+}, initial Fe^{3+}concentration=10^{-4} mol/L, adapted from (Jin, et al., 2016).

Quartz is also naturally hydrophilic but more so than hematite due to higher bond polarity (Wills, et al., 2016). Quartz has a tetrahedral crystal structure: in each unit cell, one Si atom is connected to four O atoms from the same unit cell; each O atom is connected with two Si atoms from two different unit cells (Boisen, et al., 1993; Lager, et al., 1982; Jin, et al., 2016). Due to the high bond energy of Si-O bonds, the fracture surface of quartz is expected to have a high degree of polarization (Jin, et al., 2016; Wills, et al., 2016). A schematic representation of the interaction between a freshly formed surface of quartz and water is shown in Figure 2.3. In water, the dangling Si bonds on quartz surface (as shown in Figure 2.3 (a)) can be hydrated and form SiOH groups

(Figure 2.3 (b)). These groups can interact with water molecules through hydrogen bonding, rendering the mineral surface hydrophilic (Figure 2.3 (c)) (Wills, et al., 2016).

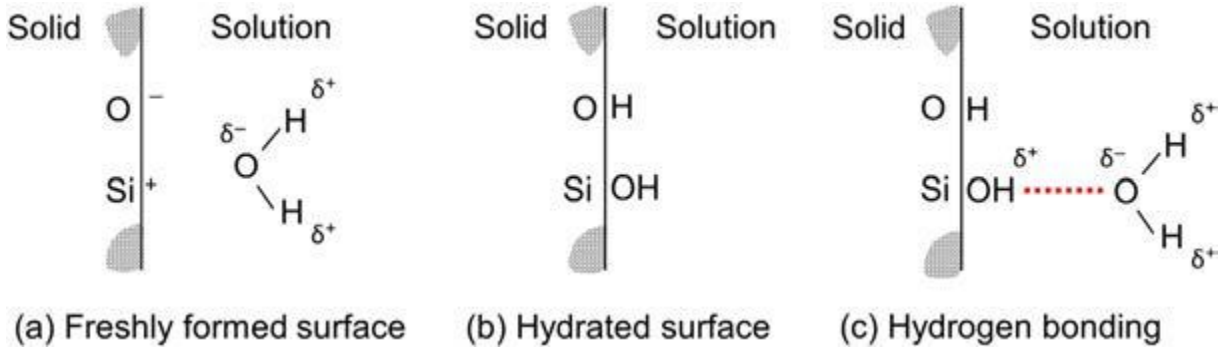

Figure 2.3. Schematic representation of the interaction between quartz surface and water, figure adapted from (Wills, et al., 2016).

2.2 REM processing

Common separation techniques for REM include gravity separation, magnetic separation, electrical separation and froth flotation (Jordens, et al., 2013). The following sections will briefly introduce them; however, the main focus will be on flotation, which is the technique most widely applied for REM processing, and, the technique that has been used in this project.

2.2.1 Gravity separation

Gravity separation separates particles based on the difference in their density. It is suitable to separate minerals with relatively high specific gravity from gangue minerals with low specific gravity (Ferron, et al., 1991; Wills, et al., 2016). For example, for REM processing, gravity separation is commonly applied to separate monazite from heavy mineral sands (Jordens, et al., 2013). The separation can be estimated by concentration criterion $\Delta\rho$, which is defined by Eq. (2.9) (Wills, et al., 2016):

$$\Delta\rho = \frac{\rho_H - \rho_F}{\rho_L - \rho_F} \qquad \text{Eq. (2.9)}$$

Where ρ_H, ρ_L, and ρ_F are the densities of heavy, light mineral, and the fluid medium respectively. The specific gravity of the minerals investigated in this project are compared as an example in Table 2.2. When $\Delta\rho$ is greater than 2.5, the gravity separation is relatively easy; when it is below 1.75, the separation becomes difficult. When $\Delta\rho$ is below 1.25, separation becomes impossible to achieve by gravity (Wills, et al., 2016). It is important to note that, in addition to density, gravity separation is also affected by particle size: generally, the efficiency of gravity separation decreases as particle size decreases (Wills, et al., 2016). This is because the movement of fine particles is controlled by their surface friction (Wills, et al., 2016). This might make gravity separation impossible to process particles with a wide range of size distribution (*i.e.* with a lot of fine particles).

Gravity separation can be further categorized into different types. Among them, jigging is one of the oldest separation techniques, which has been commonly applied to process relative coarse coal particles (Wills, et al., 2016). In some coal and iron concentrators, jigging is used to process particles larger than 150 μm (Wills, et al., 2016). It has advantages such as being less expensive than other techniques including dense medium separation (Wills, et al., 2016). However, fine particles could influence separation and therefore should be carefully controlled (Wills, et al., 2016). Spiral concentrators are another gravity separation technique, which has been widely used to process heavy mineral sand deposits (Wills, et al., 2016). Spirals are effective for processing particles in a size range of 0.1-2 mm at a capacity of 1-6 t/h (Wills, et al., 2016). Similarly, it is also sensitive to particle size and is not efficient for processing feed with a wide particle size distribution. Shaking table, another gravity separation technique, is also sensitive to particle size distribution, whose separation efficiency decreases as particles size range increases. Shaking table has a relative low throughput compared to spiral: it is able to process 0.5 t/h (for 100-150 μm feed particle size) up to 2 t/h (for 1.5 mm particle size) (Wills, et al., 2016).

Knelson and Falcon concentrators are commonly applied gravity separation techniques. They apply high centrifugal force on particles and are able to process finer particles than other gravity separation techniques (Jordens, 2016). A Knelson concentrator is able to process particles from 10 μm to 6 mm in diameter, up to 150 t/h (Wills, et al., 2016). Examples of applications of both concentrators include gold, silver, and native copper recovery (Wills, et al., 2016). Inside a Knelson concentrator (as seen in Figure 2.4 (a)), particles are trapped in the concentrating bed

inside the rotating bowl; the bed is fluidized by water to allow exchange of low-density particles with high-density ones (Wills, et al., 2016). As a result, a Knelson concentrator is capable to selectively recover dense material, which could be only a small fraction of the total feed (typically 0.01%-0.1%) (Fullam, et al., 2001). The dense materials will be flushed out from the concentrating bed periodically in order to maintain high selectivity (Fullam, et al., 2001). Previous work has investigated using Knelson and Falcon concentrators to process a RE ore from the Nechalacho deposit in Canada (Jordens, et al., 2016). Knelson concentrator was found to be capable to selectively recover larger particles that the recovery of fine particles was significantly lower than coarser ones; for particles in the 15-30 µm range, the recovery increases with respect to the specific gravity, which suggests that the Knelson concentrator is capable to selectively recover particle with higher density. However, a similar trend was not observed for Falcon concentrator in the same work. This could be due to different bowl geometry, centrifugal acceleration, and feed particle distribution between the two concentrators (Jordens, et al., 2016).

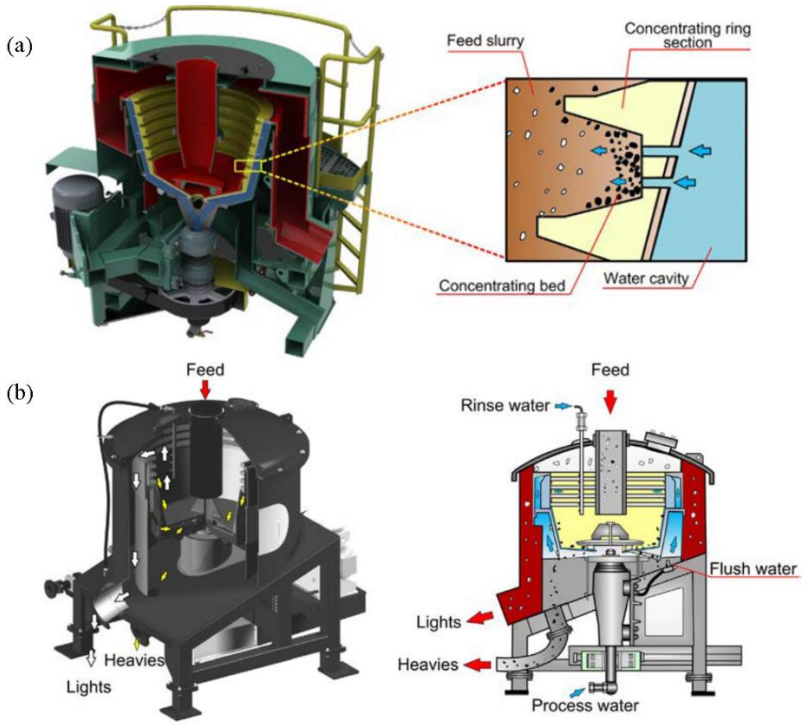

Figure 2.4. Schematic representation of (a) Knelson and (b) Falcon concentrators, adapted from (Wills, et al., 2016).

2.2.2 Magnetic separation

Compared to gravity separation, magnetic separation relies on the different magnetic properties of mineral particles. Due to unpaired electrons, minerals have different magnetic moment and respond differently in a magnetic field (Jordens, 2016). Generally, minerals can be categorized into two main groups based on their magnetism: diamagnetic and paramagnetic (Wills, et al., 2016). Diamagnetic (often referred as "non-magnetic") materials are repelled along the magnetic field lines; examples include quartz (SiO_2) (Wills, et al., 2016). In contrast, paramagnetic materials are attracted in the field along the magnetic field lines; common paramagnetic minerals include rutile (TiO_2), monazite, and xenotime (Wills, et al., 2016). Ferromagnetic materials (*e.g.* magnetite (Fe_3O_4)) is a special case under the paramagnetic category: compared to other paramagnetic materials, ferromagnetic particles can align their magnetic moment more rapidly in a magnetic field, and the force felt by ferromagnetic particles in a weak magnetic field is greater than paramagnetic particles (Jordens, 2016). The magnetic property of the minerals investigated in this project can be seen in Table 2.2. It should be noted that the magnetic response of a material does not only depend on the constituent atoms but also depends on their structure. One example is the slightly paramagnetic pyrite (FeS_2) and the strongly magnetic monoclinic pyrrhotite ($Fe_{1-x}S$), the two minerals are chemically similar to each other (Wills, et al., 2016).

Table 2.2. The specific density and magnetic property of the minerals investigated in this project, data adapted from (Jordens, et al., 2014).

Mineral	Specific gravity	Magnetic property
Quartz	2.63	Diamagnetic
Hematite	5.30	Paramagnetic
Bastnäsite	4.98	Paramagnetic

Magnetic separation has been used to recover paramagnetic REMs (such as xenotime and monazite) from diamagnetic gangue minerals, or, to reject highly magnetic gangues such as magnetite (Gupta, et al., 1992). A Frantz isodynamic separator is a lab-scale magnetic separator, which has been used in this project for separation purposes. A schematic view and an actual picture of Frantz can be seen in Figure 2.5. By applying a current on the magnetic coil, a magnetic field can be generated around a vibrating chute. Mineral particles are passed through the inclined chute, at where they receive a magnetic force, together with the force of gravity. These forces are pointing

to different directions (as described by angles $\theta_1$and θ_2 in Figure 2.5 (a)) that if the applied magnetic force is greater than its own gravity, the particle will be reported in the magnetic collection (as shown in Figure 2.5 (b)); otherwise, the particle will be reported as non-magnetic. The separation can be adjusted by changing the voltage applied on the coil, as well as by adjusting the incline angles (Wills, et al., 2016). Low- and high-intensity magnetic separators are also commonly applied. Low-intensity separators are used to recover ferromagnetic particles using a low magnetic field strength (<0.3 T) (Wills, et al., 2016). Depends on the size of feed and other factors (such as the expectation on separation), they can be designed as concurrent, counter-current, and counter-rotation types (Wills, et al., 2016). In contrast, high-intensity magnetic separators apply a strong magnetic field (>2 T) to recover weakly paramagnetic materials (Wills, et al., 2016). It should be noted that fine particles might be more difficult to recover than the coarser ones in a weak magnetic field due to the strong drag force (Jordens, 2016). Possible solutions include using a stronger magnet and adding rougher/cleaner stage(s) to improve separation (Jordens, 2016).

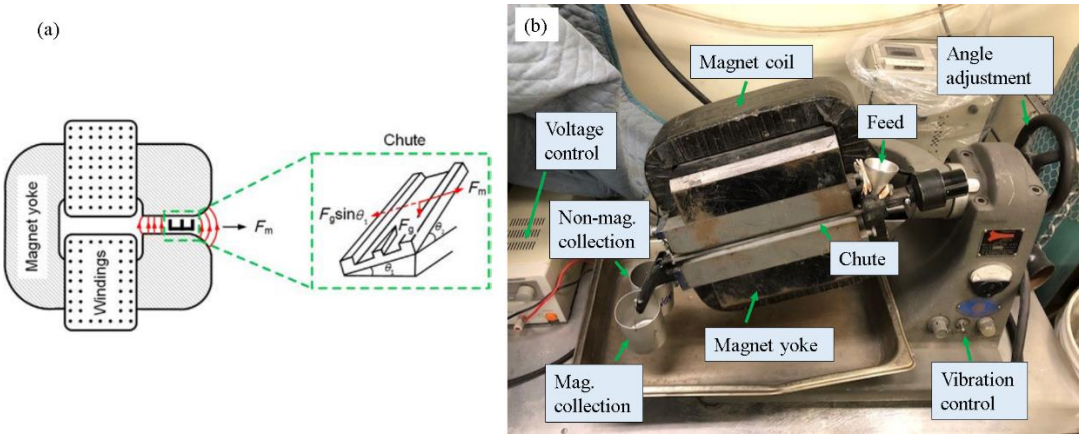

Figure 2.5. A (a) schematic representation (Wills, et al., 2016) and (b) an actual picture of a Frantz isodynamic separator.

2.2.3 Electrostatic separation

Electrostatic separation is a process that separates minerals based on their difference in conductivity; application examples include separating monazite and xenotime from gangues with similar specific gravity and magnetic properties (Jordens, et al., 2013; Higashiyama, et al., 2007). Unlike gravity and magnetic separation, electrostatic separation is a surface-based process as

charges accumulate on the particle surface (Wills, et al., 2016). A particle can be charged by three mechanisms: ion bombardment, conductive induction, and frictional (or triboelectric) charging (Wills, et al., 2016). A particle can obtain surface charge via ion bombardment in an environment of ionized gas. The charged particles are then in contact with a rotating drum, which is earthed. The nonconductive particles will stick on the drum; whereas the conductive particles will lose their charge to the earth when they are in contact with the drum and get separated from the rest. A particle can also acquire charges by conductive induction. By this method, a particle is polarized in an electric field; opposite charges will be induced at the surface of particle adjacent to the induction electrodes. The particle's response to the induced polarization is related to its own conductivity: a conductive particle is able to redistribute its charges and leave the field as non-polarized, whereas a nonconductive one will remain polarized (Wills, et al., 2016). Particles can be charged via the triboelectric mechanism based on their difference in work function, which is an electronic property of materials that measures the difference between the Fermi energy level the free electron state (Wills, et al., 2016). When two particles with different work functions are in contact, the one with higher work function will become negatively charged, and vice versa. Then, the particles can be separated between two oppositely charged electrodes (Wills, et al., 2016). In order to separate effectively, most separation units require a single layer of particles, which significantly lowers the operation capacity and makes the throughput of electrical separation low in general (Wills, et al., 2016).

2.2.4 Flotation

Flotation is the most important mineral separation technique (Wills, et al., 2016). Compared to other separation techniques, flotation has higher selectivity with lower cost, which make it more attractive for treating low-grade and complex ores (Somasundaran, et al., 2007). It can also process a wide range of particle size and can be customized for different deposits (Jordens, et al., 2013; Krishnamurthy, et al., 2005). Two of the largest REM deposits in the world, Bayan Obo (China) and Mountain Pass (USA), have successfully applied flotation to process REE ores (Zhang, et al., 2012). Separation in flotation relies on particles' surface hydrophobicity and subsequent attachment to air bubbles. This is also referred as the "true flotation" (Wills, et al., 2016). A schematic presentation of the flotation is shown in Figure 2.6. Air is injected through the shaft into

the bottom of flotation cell, which is then broken into small bubbles by an impeller. When these bubbles rise from the bottom of cell, hydrophobic particles will be attached to a bubble and carried to the froth zone. These particles are continuously collected as an over flowing froth. Meanwhile, the hydrophilic particles remain in the pulp to be pumped out (Wills, et al., 2016). Beside the "true flotation", entrainment and physical entrapment are two other ways which recover particles non-selectively (Wills, et al., 2016).

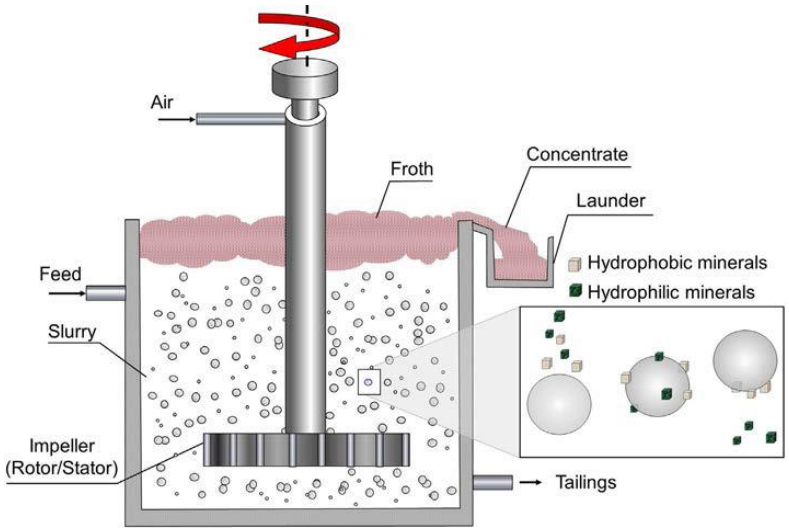

Figure 2.6. Schematic presentation of froth flotation, adapted from (Wills, et al., 2016).

As discussed above, hydrophobicity is a key factor in froth flotation. This property is a result of the surface bonding type. Polar bonds (*i.e.* strong covalent bonding, ionic bonding) are hydrophilic due to strong interactions with water molecules (Wills, et al., 2016). In contrast, non-polar bonds with relative weaker molecular bonding are naturally hydrophobic since they interact weakly with water (Wills, et al., 2016). Most minerals are naturally hydrophilic (Wills, et al., 2016); therefore, chemical reagents such as collectors and regulators are usually applied to modify the particle surface properties (Somasundaran, et al., 2007). Collectors are used to improve the surface hydrophobicity of particles, and make them "collectable" in the flotation process. They can be non-ionizing compounds (*e.g.* kerosene), which is insoluble in water and strongly hydrophobic (Wills, et al., 2016). These are commonly used to improve hydrophobicity of naturally hydrophobic minerals (such as coal) through a natural hydrophobic interaction (Wills, et al., 2016). The majority of collectors are ionizing compounds that are soluble in water. These collectors have the basic structure of a hydrophilic polar group with a hydrophobic hydrocarbon chain (as shown in Figure 2.7) (Wills, et al., 2016). The polar groups of the collector molecules adsorb onto mineral

surface; the non-polar carbon chain brings hydrophobicity to the mineral surface (Wills, et al., 2016). Collectors adsorb onto a mineral surface through two adsorption mechanisms: physical and chemical adsorption (Wills, et al., 2016). They can be driven by van der Waals forces, hydrogen bonding, and hydrophobic forces (Nagaraj, et al., 2007). Physical adsorption (or physisorption) relies on electrostatic attraction between collector and mineral surface. For example, cationic quaternary ammonium collectors adsorb on negatively charged quartz through physisorption mechanisms; the electrostatic interaction and van der Waals force are the main driven forces for their adsorption (Sahoo, et al., 2015; Wang , et al., 2005; Weng, et al., 2013). In contrast, chemical adsorption (or chemisorption) involves the formation of covalent or coordinate bonds between collector and mineral surface (Wills, et al., 2016; Somasundaran, et al., 2007; Miller, et al., 2007). Compared to physisorption, chemisorption is influenced less by the surface charge density, the functional groups, as well as the presence of inorganic ions in the pulp (Nagaraj, et al., 2007). It should be noted that a mixed adsorption mechanism could appear at the same time. In addition to these two mechanisms, other interactions including van der Waals forces, hydrogen bonding, and hydrophobic force play an important role in reagent adsorption (Nagaraj, et al., 2007).

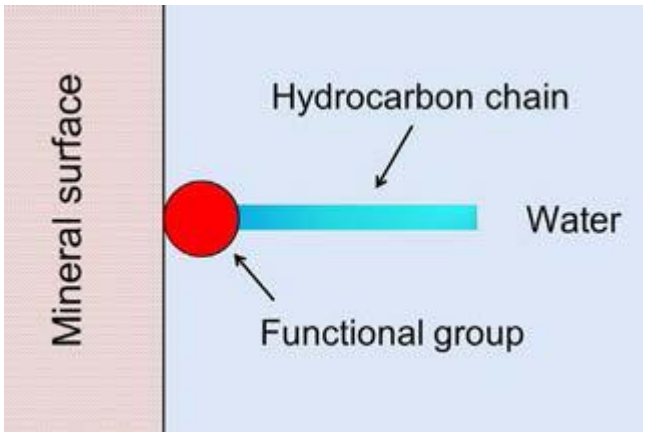

Figure 2.7. Schematic representation of a collector molecule being adsorbed onto mineral surface, adapted from (Wills, et al., 2016).

Beside collectors, other reagents including depressants, pH modifiers, and frothers are often required in froth flotation (Wills, et al., 2016). Frothers are reagents that helps form and preserve small bubbles, reduce bubble rise velocity, and aid froth formation (Wills, et al., 2016). Smaller bubbles offer a greater specific surface area for mineral particles to attach to; slower rising velocity allows more collision between bubbles and the mineral particles, which therefore facilitates the

flotation kinetics (Wills, et al., 2016). A stable froth layer allows floated particles to be recovered before the bubbles burst (Wills, et al., 2016). The general structure of a frother is very similar to that of a collector: they are comprised of a hydrophilic head and a hydrophobic chain (Wills, et al., 2016). Frothers can be categorized as aromatic alcohols, alkoxy, aliphatic alcohols, and synthetic which containing polyethylene, polypropylene, and polybutylene oxides (Pugh, 2007). Currently, over 80% of all the frothers used for metallic ore flotation fall into MIBC (a type of aliphatic alcohol) and polyglycol ether (Pugh, 2007). Depressants are used to improve the separation efficiency of flotation by selectively preventing minerals from being floated. Depressants can be categorized as inorganic, small organic, and organic polymers (Nagaraj, et al., 2007). Possible depressing mechanisms include blocking collector adsorption, adsorbing hydrophilic species, deactivating the mineral surface, and removing hydrophobic sites (Wills, et al., 2016). The following sections will be briefly reviewing common reagents applied for REM flotation.

2.2.4.1 REM flotation reagents

2.2.4.1.1 Collectors

For REM flotation, typical collectors include hydroxamates, fatty acids, dicarboxylic acids, and organic phosphoric acids (Krishnamurthy, et al., 2005). Fatty acids and hydroxamates have been applied in the flotation schemes in the Bayan Obo and Mountain Pass deposits (Fuerstenau, et al., 1982; Luo, et al., 1984; Chi, et al., 2001). However, these collectors face different problems during application. For example, fatty acids are not efficient to separate bastnäsite from gangue such as calcite, barite, and celestite which have similar flotation properties to bastnäsite (Krishnamurthy, et al., 2005). Fatty acids also require elevated temperature and large amounts of depressants in order to achieve good separation (Krishnamurthy, et al., 2005). The presence of impurity ions including Ca^{2+} and Mg^{2+} could be detrimental for flotation with hydroxamates because they can consume collectors in the pulp; low pH could lower the collecting effect of hydroxamates by preventing formation of chelating structure between hydroxamte and the mineral surface (Krishnamurthy, et al., 2005). In addition, even though hydroxamic acids have been proved to be more selective than other REM collectors such as oleate, the stability of the complex formed from hydroxamic acids and metal cations is not high enough that hydroxamates can be easily washed off from mineral surface (Bogdanov, et al., 1974). Recent studies on a commercial organic

phosphoric acid have shown promising recovery in REM flotation; however, high affinity to gangue minerals such as dolomite was also observed at the same time, which could potentially reduce the grade of concentrate at certain flotation conditions (Espiritu, et al., 2018).

2.2.4.1.1.1 Ionic liquids (ILs)

As mentioned above, current collectors for REM flotation face different problems. Therefore, it is desired to find other collectors with better performance. Ionic liquids (ILs) are salts composed of an organic cation and an organic/inorganic anion (Jungnickel, et al., 2008). They remain in a liquid state below 100 °C with negligible vapour pressure (Jungnickel, et al., 2008; Sun, et al., 2014). Common categories of ILs are imidazolium, pyrrolidinium, ammonium, and phosphonium types (Sun, et al., 2010). Due to properties such as having low vapour pressure, being non-volatile and non-flammable, ILs have been applied in electrodeposition, electro refining of metals, nonferrous metal hydrometallurgy, REEs solvent extraction process, etc. (Haerens , et al., 2009; Yang, et al., 2013; Sun, et al., 2014; Tian, et al., 2010; Sun, et al., 2010). ILs are so called “designer solvents”, which means their hydrophobicity and polarity are adjustable and possible to be tailored for a certain process (Sun, et al., 2010). However, problems still remain unsolved for ILs such as the relationship between their structure and properties are still unclear; the mechanism for ILs in mineral processing, electrodeposition and extraction of metal ions still remain unknown (Tian, et al., 2010).

ILs certainly have drawn attention in multiple research fields in recent years. In the field of mineral processing, ILs have been tested as quartz collector in iron ore flotation. The results suggest that it is possible to upgrade iron by a reverse flotation route; ILs, specifically of the quaternary ammonium type, are more effective quartz collectors than conventional collectors such as dodecylamine (Wang , et al., 2005; Sahoo, et al., 2015; Weng, et al., 2013). Multiple researches have investigated quaternary ammonium type collectors for quartz flotation (Sahoo, et al., 2015; Wang , et al., 2005; Weng, et al., 2013; Sahoo, et al., 2014; Sahoo, et al., 2015). They confirmed the adsorption of collectors on quartz regardless their structure and the carbon chain length. According to FTIR studies, the adsorption of quaternary ammonium type collectors onto quartz is likely through physisorption mechanisms including electrostatic interaction and van der Waals force since no strong chemical bonding was observed (Sahoo, et al., 2015; Wang , et al., 2005;

Weng, et al., 2013). Compared to other conventional quartz collectors such as dodecylamine, multiple quaternary ammonium collectors have proven more effective for quartz flotation (Sahoo, et al., 2015; Sahoo, et al., 2014).

Beside quartz flotation, ILs have also been investigated for REE extraction and separation, as well as REM flotation and separation. Yang et al. (2013) aimed at extracting REE from waste fluorescent lamps by solvent extraction; they compared the extractability of new REE extractants (namely N,N-dioctyldiglycol amic acid (DODGAA) and PC-88A) with the presence of an IL (1-butyl-3-methylimidazolium bis(trifluoromethylsulfonyl)imide, or $[C_4mim][Tf_2N]$). Higher selectivity for heavy REE was found for DODGAA, which could be further improved in the presence of IL. Later, it was found that Y and Eu could be stripped completely in either sulfuric or nitric acid at a concentration greater than 0.5 or 1 M. After the stripping process, about 1.4% of IL was lost which makes it possible to reuse IL for more extraction cycles (Yang, et al., 2013).

Tetraethylammonium mono-(2-ethylhexyl)2-ethylhexyl phosphonate ($[N_{2222}][EHEHP]$) has been investigated by Sun and Waters (2014) in the context of REE extraction. The results were compared with tetraethylammonium di-(2-ethylhexyl) phosphate ($[N_{2222}][DEHP]$) in order to investigate the effect of IL anion species. A schematic representation of their structures can be seen in Figure 2.8. A higher extractability was observed for $[N_{2222}][DEHP]$ than $[N_{2222}][EHEHP]$. This was explained by the presence of two ester groups in $[DEHP]^-$, whereas only one in $[EHEHP]^-$; by contributing to a stronger coordination of P=O group with REE, the extractability of $[N_{2222}][DEHP]$ is therefore higher. In contrast, the selectivity of $[N_{2222}][EHEHP]$ is higher than $[N_{2222}][DEHP]$ (Sun, et al., 2014). In the stripping ability tests, the lighter REEs (*i.e.* La^{3+}, Nd^{3+}) were found easier to be stripped than heavier ones (*i.e.* Eu^{3+}, Dy^{3+}, Er^{3+}). This was explained by weaker coordination between lighter REE and the IL.

In another study by the same researchers, it was found that RE-IL complexes formed between REE with a larger ionic radius and IL are easier to decompose (dissociate into ions) (Sun, et al., 2014). In addition, the acidity required for stripping by $[N_{2222}][EHEHP]$ was less than $[N_{2222}][DEHP]$ which can be explained by the weaker coordinating ability by P=O bond (Sun, et al., 2014). The interaction between IL and REE were studied by FTIR and XPS. Results indicated complexation between the phosphonate group and REE; the interaction between $[N_{2222}]^-$ and REE might follow a mixed mechanism of ion association and cation exchange (Sun, et al., 2014).

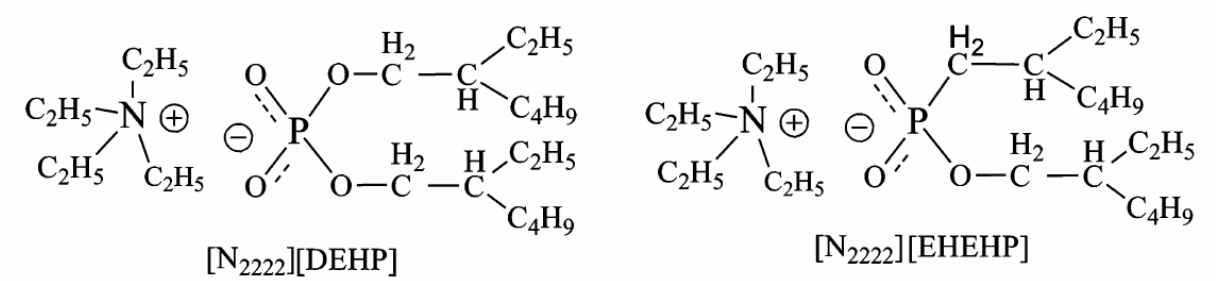

Figure 2.8. Structure of [N_{2222}][DEHP] and [N_{2222}][EHEHP], pictures adapted from (Sun, et al., 2014).

An IL with similar structure, tetrabutylam-monium bis(2-ethylhexyl)-phosphate ([N_{4444}][DEHP]), was investigated as a REM flotation collector (Azizi, et al., 2016). Researchers found that an elevated temperature was able to enhance bastnäsite recovery; this phenomenon was explained by increased mineral dissolution at higher temperature, formation of more stable re-adsorbed species, as well as the increased surface active centers (Azizi, et al., 2016). They found higher selectivity for IL towards REMs than hydroxamic acid collectors, which they explained as the formation of stronger bonding between the phosphate group in IL and REM. In their work, a decreased recovery in the alkaline pH range was observed; this was explained by the presence of $Re(OH)_3$ and $Re(OH)_4^-$ which consumes IL in the solution (Azizi, et al., 2016). FTIR results suggest the uptake of IL phosphonate moiety by forming strong chemical bond, and the interaction was stronger at pH 7 than pH 9 (Azizi, et al., 2016). Zeta potential measurement confirmed the adsorption of IL onto bastnäsite through the entire pH range. Their overall results suggest the mechanism is likely due to chemisorption (Azizi, et al., 2016).

The same IL, together with other ILs with different functional groups, have been compared for liquid-liquid REM separation (Azizi, et al., 2017). By comparing recovery results between ILs with different structures, it was found IL anions play a more important role than cations, which could be rationalized as the anions are favorable chelating groups to form ligand-RE complexes (Azizi, et al., 2017). It was found the recovery for bastnäsite was the highest in acidic near neutral pH; low recoveries were observed at pH below 4. This could be explained by preventing formation of chelation active centers such as $RE(OH)_2^+$ and $RE(OH)^{2+}$; the IL anionic moiety might also be present in molecular form at low pH which does not contribute to mineral activation and therefore no IL adsorption onto mineral surfaces (Azizi, et al., 2017). As the pH increases to between 4 and 9, the concentration of metal hydroxyl cations increases, therefore create more active sites for IL surface interactions. However, the negative zeta potential could suggest hindered interactions due

to repulsive electrostatic forces. At pH>9, negatively charged hydroxyl species such as $RE(OH)_3$ and $RE(OH)_4^-$ dominate which lower mineral recovery by repulsive forces. This was confirmed by FTIR which shows no IL peaks at pH 11. Furthermore, the more negative zeta potential also suggest strong repulsive electrostatic forces at high pH values (Azizi, et al., 2017).

In some research, micellization of ILs has been frequently discussed. IL cations and anions share a similar structure: having a hydrophilic functional group and a hydrophobic tail; this structure suggests that ILs could form a micelle structure (Łuczak, et al., 2009). The critical micelle concentration (CMC) for various types of ILs has been investigated by researchers. It was found that the value of CMC could be affected by the carbon chain length: it decreases as the chain length increases (Łuczak, et al., 2009; Geng, et al., 2010; Dong, et al., 2007; Jungnickel, et al., 2008). Micelle-micelle interaction was also observed for system with short chain length (Geng, et al., 2010). The value of CMC is also affected by the presence of other reagents. Sodium halide salts were confirmed to be able to decrease the value of CMC (Dong, et al., 2007); Chen et al. found that CMC was significantly higher in the presence of surfactant (Chen, et al., 2016). In addition, they found that IL ions could co-assemble with surfactants during micellization (Chen, et al., 2016). However, other factors such as temperature has little effect on CMC (Geng, et al., 2010).

Micellization could affect the metal ion extraction process (Visser, et al., 2002). In a study on adsorption of imidazolium type IL on kaolinite, different mechanism might be involved at different IL concentrations: at lower concentration, ion-exchange and van der Waals interactions might be the driven forces for adsorption; at higher concentration, chain-chain interaction might be the dominant adsorption mechanism (Mrozik , et al., 2008). It was also found that the micellization or bilayer formation process is more likely to happen for ILs that are less hydrophobic (*i.e.* with shorter carbon chain) (Mrozik , et al., 2008). By comparing ILs with single butyl alkyl chain with those quad-substituted, researchers found that the latter was more likely to form double-layer structure at high concentration (Mrozik , et al., 2013).

In this work, $[N_{2222}]$[EHEHP], the same IL which has shown superior extractability and selectivity as a REE extractant in Sun and Waters' work (2014), was chosen to be tested as a REM flotation collector for the first time. The structure of $[N_{2222}]$[EHEHP] (as in Figure 2.8) has collector characters such as hydrophobic groups (*i.e.* carbon chains), as well as the charged terminal atoms which might act as functional groups and might have the affinity to adsorb onto mineral surface.

It should be noticed that although [N_{2222}][EHEHP] was proved to be a selective extractant targeting on RE ions, some ILs with similar quaternary ammonium groups have been previously tested as collectors for quartz flotation (as introduced previously); its affinity to quartz might be detrimental to REM flotation.

2.2.4.1.2 Depressants

Common depressants for REM processing include sodium silicate, sodium hexafluorosilicate, lignin sulfonate, and sodium carbonate (Krishnamurthy, et al., 2005). It should be noted that the presence of depressants such as lignin sulfonate could be detrimental to REM recovery by depressing REM to a certain extent (Krishnamurthy, et al., 2005). In this project, three common depressants targeting quartz and hematite gangue minerals have been tested to improve the separation performance: sodium silicate, NorligH (a commercial depressant contains calcium lignin sulfonate), and manganese chloride. The following sections briefly review them with application examples in mineral flotation.

Sodium silicate is a common silicate mineral depressant that has been applied in many different projects. Arantes and Lima (2013) investigated sodium silicate in iron ore (hematite and goethite are main Fe-containing minerals) flotation. With sodium oleate as collector and sodium silicate as depressant, the researchers were able to upgrade the Fe content from 42% to greater than 55% with over 90% recovery. The increased sodium silicate dosage resulted a minimal change in the Fe recovery and grade (Arantes, et al., 2013). Feng et al. (2012) investigated the depressing effect of sodium silicate on lizardite ($Mg_3Si_2O_5(OH)_4$) in pyrite flotation. They found that the ore mixture could be effectively dispersed by sodium silicate, and the sliming effect of lizardite could be decreased by sodium silicate in a wide pH range (from 6.2 to 11). Based on speciation and XPS studies, researchers concluded that $SiO(OH)_3^-$ is the predominant species that adsorbs onto lizardite within the tested pH range (Feng, et al., 2012). Billinghurst (1951) investigated the depressing effect of sodium silicate on quartz in pyrite flotation with the presence of sodium oleate and terpineol as collectors. It was found that the recovery of quartz decreased more than pyrite as the dosage of sodium silicate increased from 0 to 50 mg per test (equivalent to 1 kg per ton of feed). Sodium silicate was considered to be more effective than other quartz depressants including sodium chloride and sodium sulphate, since its dosage required to reach the same depressing effect

was lower (Billinghurst, 1951). The depressing mechanism proposed was likely due to the presence of both sodium ions and silicate ions (Billinghurst, 1951). Jin et al. (2016) found that the presence of Fe^{3+} ions activated quartz by interacting with the Si-O groups. Sodium silicate covers these activated sites, and prevent anionic collectors from being adsorbed (Jin, et al., 2016). The same adsorption mechanism was also suggested by Silva et al. (2012), who investigated the depressing effect and mechanism of sodium silicate for calcite and quartz with the presence of an amine collector. They found that the species in sodium silicate solution are a collection of monomeric and polymeric species, as well as colloidal silica SiO_2. Researchers found that the best depressing performance was at pH 5-8; at pH 7, SiO_2 and $Si(OH)_4$ were the dominant species detected on the mineral surface, whereas at pH 11, no adsorption of sodium silicate on mineral was detected. From their investigation, the proposed adsorption mechanism was by sharing electron pairs between Si-O sites of the mineral and the silicate species (Silva, et al., 2012).

Sodium silicate has also been tested in floating other ore types. It has been investigated as a silicate depressant in molybdenite ore flotation (Park, et al., 2010). It was found that sodium silicate was able to increase pH, prevent slime coating, and depress quartz. The proposed depressing mechanism was $HSiO_3^-$ and SiO_3^{2-} creating a stable dispersion between particles and repulsion between anionic collector species and particles (Park, et al., 2010). Sodium silicate has also been applied in bitumen flotation to precipitate Ca^{2+} and Mg^{2+}; this prevents clay coating bitumen, maintains pH for flotation, and disperses/depresses fine clay particles (Li, et al., 2005).

To study the silicate species at different pH, Jin et al. (2016) summarized the balance equations and their equilibrium constants as following:

$$SiO_2 + 2H_2O \rightleftharpoons Si(OH)_4 \qquad K_s = 2.00 \times 10^{-3} \qquad \text{Eq. (2.10)}$$

$$SiO_2(OH)_2^{2-} + H^+ \rightleftharpoons SiO(OH)_3^- \qquad K_1 = 3.63 \times 10^{12} \qquad \text{Eq. (2.11)}$$

$$SiO(OH)_3^- + H^+ \rightleftharpoons Si(OH)_4 \qquad K_2 = 2.69 \times 10^{9} \qquad \text{Eq. (2.12)}$$

Based on these equations, an ion speciation diagram was drawn with an initial sodium silicate concentration of 10^{-4} mol/L (as shown in Figure 2.9). It can be observed that the predominant ion specie at pH<7 is $Si(OH)_4$; as pH increases to 7-12, $SiO(OH)_3^-$ is considered as majority. As pH further increases, $SiO_2(OH)_4^{2-}$ becomes dominant in the system.

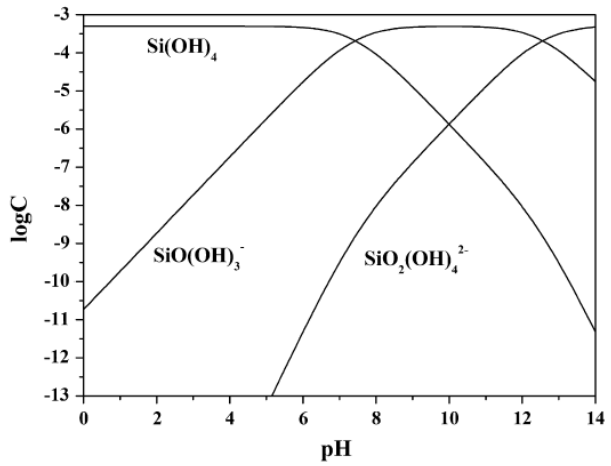

Figure 2.9. Silicate ion speciation diagram with initial sodium silicate concentration 10^{-4} mol/L, adapted from (Jin, et al., 2016).

Lignin sulfonate is another common silicate depressant, which is a natural product and derivative belongs to the category of organic polymers (Pugh, 1989; Bulatovic, 1999). It can be associated with different metal cations to form compounds; one commonly applied is calcium lignin sulfonate (Pugh, 1989; Bulatovic, 1999). The adsorption of lignin sulfonate, among other organic depressants, is influenced by hydrophobic interactions, electrostatic interactions, hydrogen bonding, and chemical interactions (Pugh, 1989; Bulatovic, 1999).

Lignin sulfonates have been tested in flotation for different ore bodies. Ansari (2003) compared the depressing effect of lignin sulfonates on molybdenite and chalcopyrite. It was found that the adsorption of lignin sulfonates can be enhanced by activating the mineral surface with polyvalent cations such as calcium (Ansari, 2003). Due to this reason, applying lime as a pH modifier was not recommended by the researchers since Ca^{2+} can activate both molybdenite and chalcopyrite non-selectively (Ansari, 2003). The adsorption mechanism for anionic lignin sulfonates at alkaline pH was proposed to involve electrostatic forces (Ansari, 2003). Marion et al. (2015) were able to separate muscovite from quartz by froth flotation with calcium lignin sulfonate as a depressant for quartz, and an amine as collector. At a 250 g/t collector dosage and a 1500 g/t depressant dosage, the recovery of quartz was as low as 15%, and effective separation was achieved for the mica-quartz ore. Zhu et al. (2015) investigated calcium lignin sulfonate as quartz depressant with the presence of Fe^{3+} ion. It was found that Fe^{3+} could adsorb onto the quartz surface and activate quartz at pH 3; this resulted in identical flotation response for quartz and other valuable minerals. The

addition of calcium lignin sulfonate could effectively depress quartz and achieve selective separation (Zhu, et al., 2015).

Manganese chloride ($MnCl_2$) has been reported as a depressant for hematite and quartz in the presence of an amine collector (Lelis, et al., 2016). Researchers concluded that the depressing effect of $MnCl_2$ could be due to adsorption of positively charged Mn species (including Mn^{2+}, $Mn_2(OH)^{3+}$, and $Mn(OH)^{+}$) as well as precipitation of $Mn(OH)_2$. These species hinder the adsorption of amine molecules and prevent minerals from being floated (Lelis, et al., 2016). It was also found that $MnCl_2$ depresses hematite more than quartz. This was rationalized by the formation of cationic chlorocomplex on hydrated iron oxide and the decreased electrostatic forces between hematite and amine molecules (Lelis, et al., 2016).

To study the manganese ion speciation in an aqueous system, the hydrolysis reactions of Mn ion species in water at 25 ºC have been summarized by Lelis et al. (2016):

$$Mn^{2+} + OH^{-} \rightleftharpoons Mn(OH)^{+} \qquad \log K_1 = 3.4 \qquad \text{Eq. (2.13)}$$

$$Mn^{2+} + 4OH^{-} \rightleftharpoons Mn(OH)_4^{2-} \qquad \log K_2 = 7.7 \qquad \text{Eq. (2.14)}$$

$$2Mn^{2+} + OH^{-} \rightleftharpoons Mn_2(OH)^{3+} \qquad \log K_3 = 3.4 \qquad \text{Eq. (2.15)}$$

$$2Mn^{2+} + 3OH^{-} \rightleftharpoons Mn_2(OH)_3^{+} \qquad \log K_4 = 18.1 \qquad \text{Eq. (2.16)}$$

$$Mn(OH)_{2(s)} \rightleftharpoons Mn^{2+} + 2OH^{-} \qquad \log K_5 = -12.8 \qquad \text{Eq. (2.17)}$$

Based on these equations, a speciation diagram was drawn by Lelis et al. (2016) (as shown in Figure 2.10). The predominant ion species at pH below 4.5 is $Mn_2(OH)^{+}$; at pH between 4.5 and 8.5, the majority ion is Mn^{2+}. As pH further increases to 13, the predominant ions become $Mn_2(OH)^{3+}$. At the tested condition (pH 10.5) in literature, the predominant ion species are $Mn_2(OH)^{3+}$, with Mn^{2+} and $Mn(OH)^{+}$ in the aqueous system (Lelis, et al., 2016).

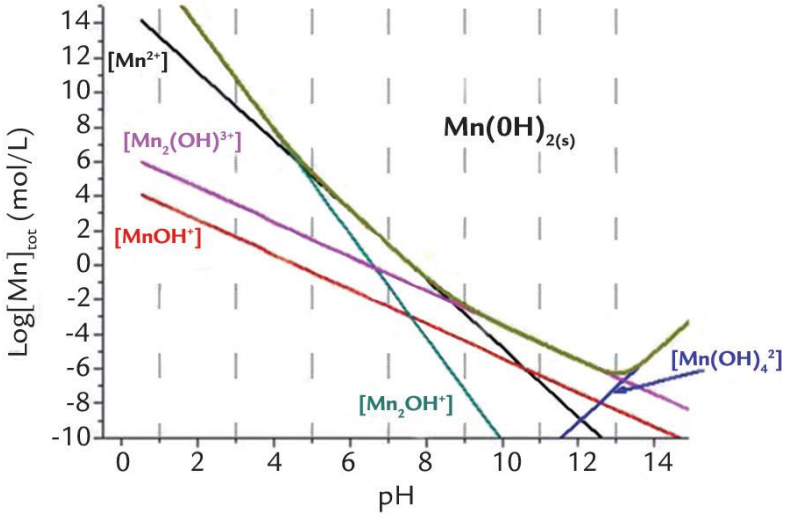

Figure 2.10. Mn ion speciation diagram at 25 ºC, adapted from (Lelis, et al., 2016).

2.2.4.2 Flotation surface chemistry

In this project, zeta potential and Fourier transform infrared spectroscopy (FTIR) techniques were used to analyze the adsorption of IL onto mineral surface. The same techniques have been effectively applied for similar purposes (Sahoo, et al., 2015; Sahoo, et al., 2014; Azizi, et al., 2016; Azizi, et al., 2017). Microflotation, as a technique that could mimic a certain flotation condition (*i.e.* reagent dosage, pH) and test the mineral's response, has also been widely applied in studies on mineral flotation. The following sections detail these techniques.

2.2.4.2.1 Zeta potential

Mineral particles in suspension can be naturally charged by the following mechanisms: ionization of surface groups, ion adsorption, ion dissolution, and isomorphous substitution (Cosgrove, 2005). The surface groups of a particle can be ionized (*e.g.* protonation or deprotonation) in an aqueous system; this process is controlled by solution pH (Cosgrove, 2005). A particle surface could also be charged by adsorbing ionic surfactants from surrounding medium (Mackenzie, 1971; Cosgrove, 2005). Change in pH could also influence the ion adsorption process. Charges can also be introduced on particle surface by dissolving ionic species (Mackenzie, 1971; Cosgrove, 2005). In addition, an atom in the lattice could be replaced by another atom of a similar size. This process is called isomorphous substitution, and can introduce charges when the replacing and substituting

atoms have different valence electrons (Cosgrove, 2005). For oxide minerals (such as quartz and hematite), the surface charge is usually a result of hydrolysis reactions and dissociation of surface hydroxyl groups, whereas for salt type minerals (such as bastnäsite), the surface charge is usually linked to surface lattice ion dissolution, hydrolysis reaction of the dissolved species, and adsorption of hydrolyzed ion species (Somasundaran, et al., 2007).

As a particle is dispersed in a liquid, a layer of reverse charge (namely the Stern layer) will be introduced immediately, which is closely attracted to the surface of the particle (Kaszuba, et al., 2010). A more loosely bonded layer (namely the diffuse layer) will also be introduced as an outer layer, which will not be stable when the particle moves in the suspension (Kaszuba, et al., 2010). These two layers are collectively called the electrical double layers; the boundary between them is the plane of shear (also named as the slipping plane, as seen in Figure 2.11) (Kaszuba, et al., 2010). The electrical double layer balances the electrical inhomogeneity between the solid particle and the suspension (Fuerstenau, et al., 2005). The electrical double layer plays an important role in flotation: the physisorption process is controlled by the sign and magnitude of surface charge (Fuerstenau, et al., 2005). Even though some reagents can be chemically adsorbed onto a mineral surface regardless the sign of charge, the adsorption could still be hindered by high surface charge (Fuerstenau, et al., 2005). The electrical double layer also governs other phenomena such as the flocculation and dispersion of a mineral suspension, as well as fine particle/air bubble interactions (Fuerstenau, et al., 2005).

To further study the electrical double layer, the concept of zeta potential was introduced. Zeta potential is the electrical potential at the plane of shear (Mackenzie, 1971) (as seen in Figure 2.11), which governs the electrostatic interactions in the dispersion (Kaszuba, et al., 2010). Zeta potential could help understand the adsorption mechanism of reagents, and aid selecting the optimum operating conditions (Fuerstenau, et al., 2005; Pope, et al., 1973). Some researchers claim that zeta potential measurement is more useful in systems involving electrostatic interactions than those involving chemisorption (Nagaraj, et al., 2007). An important factor to characterize the electrical double layer is the isoelectric point (IEP); by definition, IEP is the pH at which zeta potential is zero (Pope, et al., 1973). The IEP is helpful in predicting the sign of charge of a mineral in a given pH range (Pope, et al., 1973; Parks, 1967). By measuring zeta potential and observing the changes in zeta potential as well as the shift of IEP after addition of a certain reagent, one can predict

whether the reagent is adsorbed onto the particle surface by measuring the zeta potential is changed by an appreciable amount. This is explained schematically in Figure 2.11, which compares the zeta potential with and without the presence of external ion species. As shown in Figure 2.11 (b), the addition of metal cations (Ca^{2+}) could decrease the absolute value of zeta potential (shown as an upward shift); at some point, the value of the zeta potential could be deceased to zero (Wills, et al., 2016).

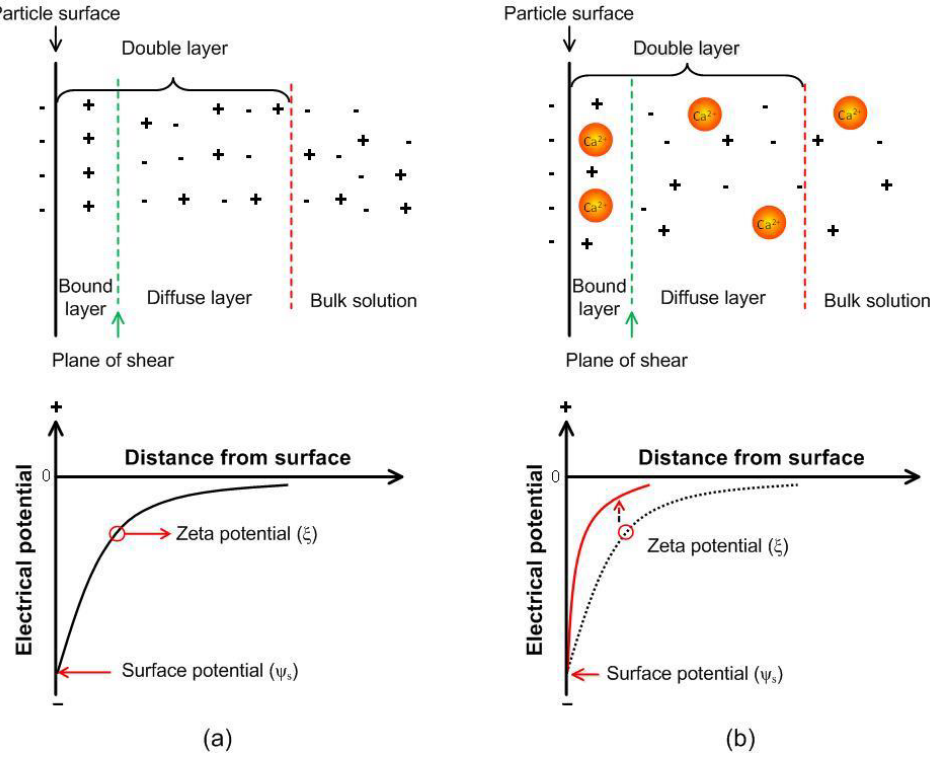

Figure 2.11. Schematic representation of zeta potential with/without additional ion species, adapted from (Wills, et al., 2016).

The zeta potential can be measured by techniques including streaming potential, electro-osmosis, electrophoresis, and electroacoustics techniques (Cosgrove, 2005). Among them, the electrophoresis and electroacoustics ones have been the most frequently applied in various literature. Electroacoustics has lower restrictions on the suspension; it is suitable for a suspension with a wide range of solid content (0.1-50 vol%) (Miller, et al., 1991). In contrast, electrophoresis requires a dilute suspension (<0.01 vol%), and is only practicable for particles with specific optical properties and size (Miller, et al., 1991; Kaszuba, et al., 2010; Babchin, et al., 1989). In case size reduction destroys the integrity of sample, electrokinetic streaming method might be a better option than electrophoresis (Johnson, 1999).

Electrophoresis has been successfully applied in many zeta potential measurement tasks, including those investigated the same minerals as this project (dos Santos, et al., 2007; Lelis, et al., 2016; Jordens, et al., 2014). In an electrophoretic zeta potential equipment, a pair of electrodes create a known electric field in the suspension. Charged particles in the field will move towards the electrode with opposite charge. A light scattering unit is applied in the cell in order to measure the velocity of particles. This is expressed as electrophoretic mobility, which is then converted to zeta potential through a series of calculations (Kaszuba, et al., 2010). A more detailed introduction about an electrophoretic zeta potential analyzer is presented as supplemental material in the Appendix.

2.2.4.2.2 Microflotation

Due to the limitation in mineral samples and reagents, microflotation has been commonly used to investigate a mineral's response at certain flotation conditions. In this work, all the microflotation tests were done in a modified Patridge-Smith cell. A schematic representation and picture of the cell are shown in Figure 2.12. In a modified Patridge-Smith cell, compressed air passes through a frit at the bottom of cell while operating; the frit is designed in a way that it allows air to pass through but the suspension will not leak out. A magnetic stirring bar is used to keep particles suspended in the cell. It should be noted that in this work, no effect of magnetic field (*e.g.* particles stick on the stirring bar or at the bottom of cell) was observed. As air bubbles rise in the cell, hydrophobic particles will attach onto bubble surface and reported in the froth zone, whereas the hydrophilic ones will stay in the pulp. The froth will be scraped from the top of column into the launder, which will be collected as concentrate. After each test, those particles left in the cell will be collected as tailings.

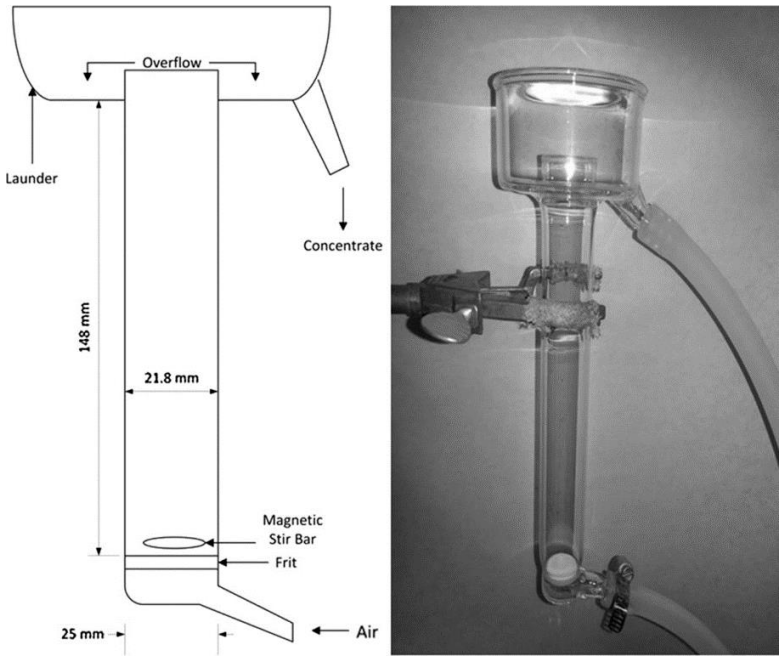

Figure 2.12. Schematic structure and photo of microflotation column, adapted from (Jordens, et al., 2014).

2.2.4.2.3 Fourier transform infrared spectroscopy (FTIR)

FTIR is employed in this project to investigate the type of bonding present on the mineral surface. This section will be briefly introducing this technique, together with some example applications in mineral processing.

Infrared (IR) spectroscopy is a technique that measures the transitions between molecular vibrational levels as a result of IR radiation absorption (Larkin, 2011); it detects molecular vibrations and identifies chemical bonds by producing an IR absorption spectrum and comparing it with database. Functional groups and their corresponding vibrations are identified by their characteristic absorption bands (Colthup, et al., 1990; Griffiths, et al., 2007). For a sample to be IR active (*i.e.* absorbs IR radiation), a change in the dipole moment must be present within the molecule during vibration. This allows molecules with asymmetric vibrations to be detected (Berthomieu, et al., 2009). Permanent dipoles (*e.g.* polar bonds) contribute to strong IR absorptions (Berthomieu, et al., 2009). This lack of selectivity of detection allows nearly all chemical groups in the sample to be detected at the same time (Berthomieu, et al., 2009). In contrast, symmetric vibrations are usually IR inactive (Berthomieu, et al., 2009). For instance, for a molecule with a center of symmetry, all vibrations that are symmetrical with respect to the center are IR inactive

(Berthomieu, et al., 2009). A more detailed introduction on IR spectroscopy is offered as supplemental material in the Appendix.

With an extensive use of IR spectroscopy in quantitative and qualitative analysis, FTIR has been developed to allow conversion of intensity-time spectrum to an intensity-frequency spectrum with greater IR interpretation (Larkin, 2011). This technique has been successfully used in mineral processing in order to investigate the adsorbed reagent species and the adsorption mechanism (Azizi, et al., 2016; Fornasiero, et al., 1995). Researchers used FTIR to study the adsorption of an IL, tetrabutylammonium bis(2-ethylhexyl)-phosphate ([N_{4444}][DEHP]), onto a mineral surface (Azizi, et al., 2016). Bastnäsite, monazite, and calcite were conditioned with [N_{4444}][DEHP] solution at pH 7 and 9 before being filtered and rinsed by water, and followed by drying in a vacuum oven at room temperature before FTIR analysis. The resultant spectra of bastnäsite and calcite are compared in Figure 2.13 and Figure 2.14. Peaks at 873, 1026, and 1415 cm^{-1} in bastnäsite spectrum were assigned to CO_3^{2-} vibration; these peaks were slightly shifted to lower wavenumbers after IL treatment (as shown in Figure 2.13). Vibrational bands at 2855.6, 2925 and 2956 cm^{-1} in IL were assigned to C-H stretching of $-CH_3$ and $-CH_2$- groups in the alkyl chains (Azizi, et al., 2016). Peaks at 1380 cm^{-1} and 1462 cm^{-1} were associated with bending bands of the same groups (Azizi, et al., 2016), whereas band at around 1180 cm^{-1} is due to P=O stretching in the phosphate moiety of the IL (Azizi, et al., 2016). The bands for IL-treated bastnäsite at pH 7 exhibited higher intensity than at pH 9, which suggests more collector adsorption at pH 7. However, these characteristic bands were not observed in the spectra for treated calcite (as in Figure 2.14 (c) and (d)). This suggests no IL adsorption on the calcite surface at the tested conditions. Bands for N-H stretching in the quaternary amine moiety, usually located at 1600-1400 cm^{-1}, were not observed in the spectra, which might suggest weak adsorption for the cationic group (Azizi, et al., 2016).

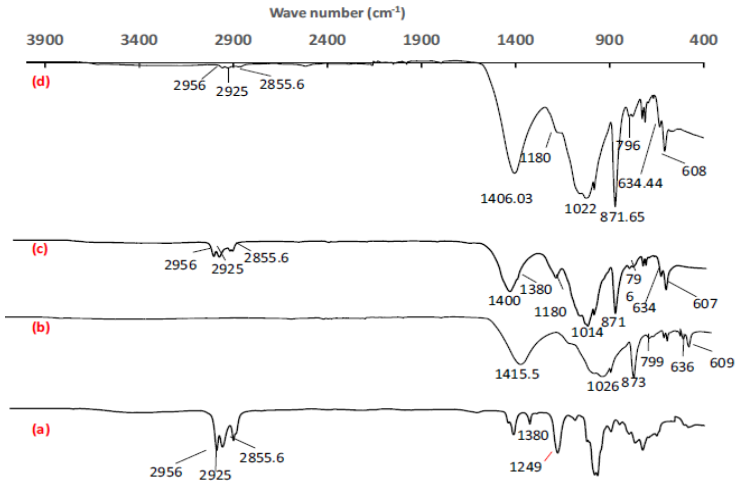

Figure 2.13. FTIR spectra of (a) [N_{4444}][DEHP], (b) bastnäsite, (c) bastnäsite after IL treatment at pH 7, and (d) pH 9, adapted from (Azizi, et al., 2016).

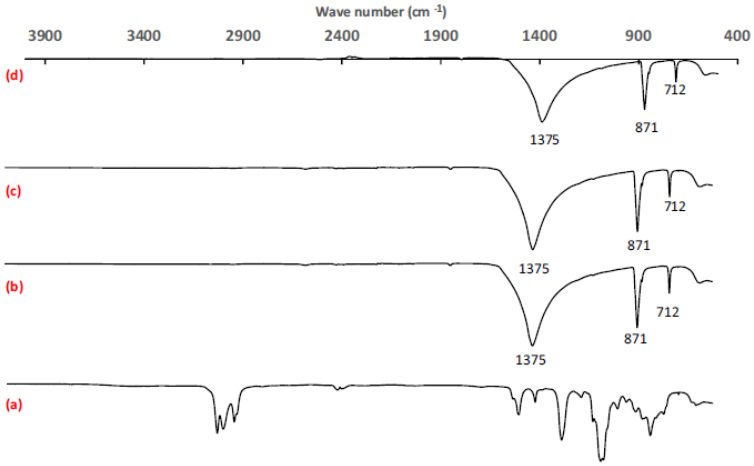

Figure 2.14. FTIR spectra of (a) [N_{4444}][DEHP], (b) calcite, (c) calcite after IL treatment at pH 7, and (d) pH 9, adapted from (Azizi, et al., 2016).

2.3 Mineral characterization

2.3.1 X-ray Diffraction (XRD)

XRD is a technique that analyzes material properties, and has been intensively used to check the phase of material prior to use (Clearfield, et al., 2008). Compared to other characterization technique, XRD has advantages such as being rapid and non-destructive to the sample (Clearfield, et al., 2008). XRD is able to identify crystalline phases quickly, and is capable of analyzing samples under a condition (*e.g.* temperature, pressure, and relative humidity) that is changing

(Clearfield, et al., 2008). In addition, due to the fact that each crystal structure has its unique spectrum, XRD is able to handle a sample with multiple components (Clearfield, et al., 2008). However, other techniques might be required beside XRD in order to validate the results; common ones include Scanning Electron Microscope (SEM) and X-ray Fluorescence Microscopy (XRF) (Clearfield, et al., 2008).

In a bulk of material, atoms are arranged in a way that they are located in planes that are parallel to each other. When X-ray interacts with the atoms, it will diffract following Bragg's law as shown by Eq. (2.18) (Clearfield, et al., 2008):

$$n\lambda = 2dsin\theta \qquad \text{Eq. (2.18)}$$

where θ is the incident angle between X-ray and the plane, d is the interlayer spacing, λ is the wavelength of X-ray, and n is an integer. As d serves as a unique property of crystal, the result X-ray spectrum will therefore be able to identify the material (Clearfield, et al., 2008).

Chapter 3. Experimental methods

3.1 Mineral sample preparation and characterization

In this project, mineral samples of bastnäsite (Madagascar), quartz (Daubois, Canada), and hematite (Québec Cartier Mining Company, Canada) were stage pulverized to produce a -106 +38 µm fraction, following a size distribution shown in Table 3.1. Bastnäsite and quartz were used without further processing, while hematite was further purified to reject quartz impurity with a Frantz isodynamic separator (Frantz, USA, as shown in Figure 2.5 (b)). Representative samples were examined by XRD using a Bruker D8 Discovery X-Ray Diffractometer (Co Kα source, λ = 1.79 Å). The resulting patterns were analyzed by Xpert High Score software (PANalytical). All samples were confirmed pure as shown in Figure 3.1.

Table 3.1. Size distribution of minerals used in microflotation tests.

	-106 +75 µm (%)	-75 +53 µm (%)	-53 +38 µm (%)	d_{50} (µm)	d_{80} (µm)
Quartz	52.63	34.30	13.07	76.6	94.2
Hematite	48.04	33.13	18.83	73.7	93.1
Bastnäsite	52.20	28.90	18.90	76.3	94.1

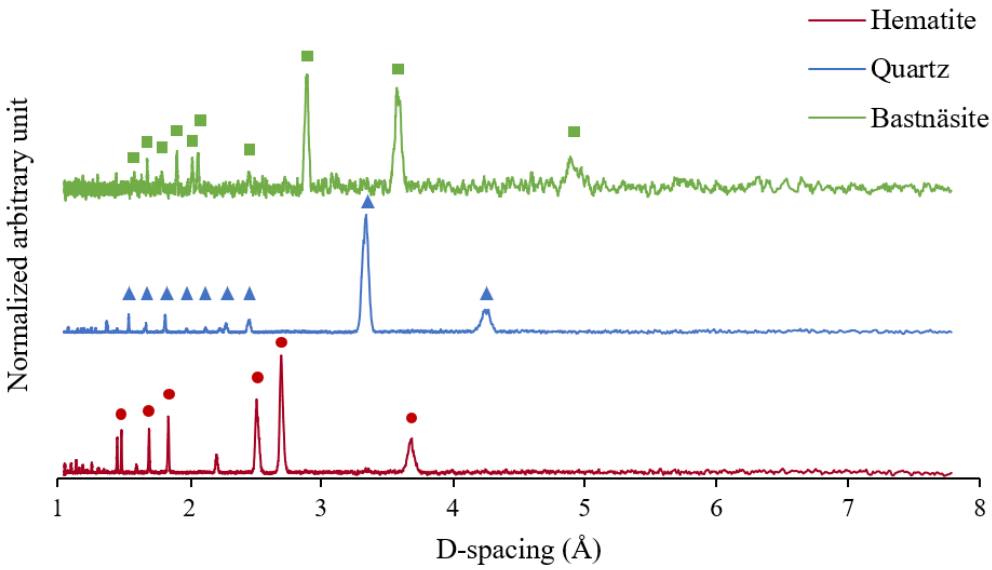

Figure 3.1. XRD spectra of bastnäsite, quartz, and purified hematite used in this project.

To prepare samples for zeta potential measurements and FTIR analysis, the –38 µm size fraction produced from stage pulverizing were wet ground for 60 min at 500 rpm using a Pulverisette 6 planetary monomill (Fritsch, Germany). Particle size was determined using a LA-920 particle size analyzer (Horiba, Japan). Their surface area was determined by nitrogen Brunauer–Emmett–Teller (N_2-BET) technique using a TriStar Surface Area and Porosity Analyzer (Micromeritics, USA). The results are shown in Table 3.2.

Table 3.2. Particle size and surface area of mineral samples used for zeta potential and FTIR analysis.

	d_{50} (µm)	Surface area (m^2/g)
Quartz	3.85	4.6905
Hematite	7.95	0.6647
Bastnäsite	2.30	11.3635

3.2 IL synthesis

Two batches of IL $[N_{2222}][EHEHP]$ were synthesized following the procedure described in previous work (Sun, et al., 2014). Raw materials tetraethylammonium chloride ($[N_{2222}]Cl$) and 2-ethyl(hexyl) phosphonic acid mono-2-ethylhexyl ester (HEHEHP) were purchased from Sigma Aldrich (USA) and supplied by Dr. Xiaoqi Sun respectively. A solution of $[N_{2222}]OH$ in ethanol was prepared from 0.9942 g of $[N_{2222}]Cl$ (0.006 mol) using Dowex Monosphere 550A (OH) anion-exchange resin. The drained solution was mixed with 1.8385 g of HEHEHP (0.006 mol), which

was then stirred at room temperature for 6 h until the solution became neutral. The ethanol and water were then distilled off by a IKA RV10 rotary evaporator, and the product was dried at 70 ˚C in a vacuum oven for 12 h to yield the final product. The products were analyzed by ^{1}H and ^{13}C nuclear magnetic resonance spectroscopy (NMR) in $CDCl_3$ background solvent with a Bruker AV III 400HD NMR spectrometer (USA). The peaks identified from the spectra are detailed below; by comparing the results with the those presented in (Sun, et al., 2014), it can be concluded that the products have the same structure as previous work, with traceable amount of water impurity in batch 1. Small shifts in the peaks might be due to water content, temperature fluctuation, and pH effect.

IL batch 1:

^{1}H NMR ($CDCl_3$, ppm): 0.83−0.93 (m, 12H, $4CH_3$), 1.39-1.43 (m, 12H, $4CH_3$), 1.24-1.57 (m, 16H, $8CH_2$), 1.37 (m, 2H, 2CH), 3.44 (m, 8H, $4NCH_2$), 3.56 (m, 2H, CH_2), 3.72 (m, 2H, OCH_2). 3.066 (H, H_2O)

^{13}C NMR ($CDCl_3$, ppm): 7.72 ($4CH_3$), 10.42 (CH_3), 11.06 (CH_3), 14.14 (CH_3), 14.24 (CH_3), 23.17 (CH_2), 23.40 (CH_2), 26.62 (CH_2), 28.70 (CH_2), 29.12 (CH_2), 30.18 (CH_2), 30.50 (CH_2), 31.83 (CH_2), 33.79 (CH_2), 34.74 (CH), 40.61 (CH), 52.65 ($4NCH_2$), 66.14 (OCH_2).

IL batch 2:

^{1}H NMR ($CDCl_3$, ppm): 0.853-0.910 (m, 12H, $4CH_3$), 1.352 (m, 12H, $4CH_3$), 1.16−1.18 (m, 16H, $8CH_2$), 1.37 (m, 2H, 2CH), 3.394 (m, 8H, $4NCH_2$), 1.706 (m, 2H, PCH_2), 3.666 (m, 2H, OCH_2).

^{13}C NMR ($CDCl_3$, ppm): 7.64 ($4CH_3$), 10.41 (CH_3), 11.05 (CH_3), 14.14 (CH_3), 14.24 (CH_3), 23.17 (CH_2), 23.39 (CH_2), 26.58 (CH_2), 28.71 (CH_2), 29.11 (CH_2), 30.19 (CH_2), 30.59 (CH_2), 31.92 (CH_2), 33.81 (CH_2), 34.81 (CH), 40.63 (CH), 52.56 ($4NCH_2$), 66.12 (OCH_2).

3.3 Microflotation

In this project, [N_{2222}][EHEHP] was tested at a low (50 g/t) and a high concentration (500 g/t) at pH 3, 5, 7, and 9. All depressants were tested at 500 g/t dosage. Microflotation tests were conducted on three model minerals in a modified Partridge-Smith flotation cell (shown in Figure 2.12). In each test, 1 g of pure mineral was allowed to condition in 30 mL collector solution at desired concentration and pH for 1 min. In case of a test with depressant, the mineral was first conditioned for 1 min in depressant solution with desired concentration prior to adding collector. A stirring bar at 1150 rpm was used to keep particles suspended during conditioning stage. After the conditioning stage, the suspension was transferred into the micro-flotation cell and the cell was filled with an additional 33 mL of pH-adjusted reverse osmosis (RO) water. Two drops of F-150 frother (obtained from Flottec, USA) solution at a concentration of 10 mg/mL was added prior to connecting the cell with air. During the tests, the airflow was set at 36 mL/min, and froth was collected by a scraper into the launder for 1 min. After each test, mineral particles remained in the cell were collected as tailing. Concentrates and tailings were collected and dried separately in order to calculate the recovery. Hydrochloric acid and sodium hydroxide used for pH modifications in this project were purchased from Fisher Scientific (USA).

3.4 Zeta potential

Zeta potential measurements were conducted using a NanoBrookZetaPlus electrophoretic analyzer (Brookhaven Instruments, USA). Mineral samples were suspended in 200 mL of 10^{-3} mol/L KCl at a mineral/solution ratio of 0.04 %w/w. The suspension was well dispersed by an ultrasonicater (Hielscher UP400S) for 30 s. A magnetic stirring bar was used to keep particles suspended through the test. The pH range investigated was from pH 3 to 10 due to equipment limitation. Prior to taking a measurement, the suspension was allowed to condition for 30 min after the addition of collector, and for minimum of 5 min at each different pH level. Fresh samples were prepared for acidic and basic zeta potential measurements to avoid zeta potential hysteresis effects. For cases with reagent (*i.e.* [N_{2222}][EHEHP] and depressants), the reagent was added into the KCl solution during the conditioning stage. Its concentration was determined by increasing the collector dosage until an appreciable shift in the bastnäsite zeta potential was observed. This concentration was then kept constant on a gram-per-ton (g/t) basis for quartz and hematite. The obtained zeta potential

data were then treated by Stata 13 statistical software in order to produce confident intervals. Detail explanation on how the software works are available in (Marion, et al., 2015).

3.5 FTIR

To prepare samples for FTIR analysis, the same mono milled mineral for zeta potential measurement was used as starting material. An amount of 0.15 g of mineral sample was first transferred into 25 mL of IL solution ([N_{2222}][EHEHP] dosage: 100 kg/t, or equivalently 2.4×10^{-4} mol/g). The suspension was dispersed using an ultrasonicater (Hielscher UP400S) for 30 s. The pH of suspension was then adjusted by diluted HCl and NaOH while a stirring bar was used to keep particles suspended at 500 rpm. The particles were allowed to condition for 15 min with pH being constantly adjusted. After conditioning, the particles was poured onto a filter paper before being rinsed with pH-adjusted RO water thrice. The samples were dried in air for 24 hours before being transferred into a vacuum over for 8 hours to dry completely. The samples were stored in a desiccator before analysis. The desiccator was filled with drierite, which was able to offer an environment with relative humidity at 0.5%. A Spectrum 400 FT-IR/FT-NIR spectrometer (Perkin Elmer, USA) was used for FTIR studies. Each spectrum was obtained from 64 scans at 4 cm^{-1} resolution in the 4000–650 cm^{-1} region. The obtained spectra were baseline corrected and normalized to the total surface area under the transmittance bands using PerkinElmer Spectrum software (Perkin Elmer, USA).

3.6 Bench scale flotation

A synthetic mixture of three minerals was tested in bench scale flotation. This aims to mimic a reverse flotation process that upgrades bastnäsite, potentially from concentrates produced by rougher flotation. Flotation experiments on the synthetic mixture were carried out in a 1.2 L Denver flotation cell at an air flow rate of 3 L/min with the impeller set at 800 rpm. For each test, 50 g of solids was prepared by mixing 16.67 g of each mineral; the mixture was transferred directly to the flotation cell where the pulp level was adjusted to a set height by adding RO water. Diluted HCl and NaOH solutions were used to adjust pH. The slurry was then allowed to condition for 1

min with depressant, followed by another 1 min conditioning stage with IL. After conditioning, 1 drop of F-150 frother was added prior to turning on the air. Froth was collected after 0.5 min, 1.5 min, 2.5 min, and 3.5 min cumulative time to produce four different concentrates. Throughout each flotation test, the water level and pH were continuously adjusted. The concentrates were then weighed, filtered, and dried in a lab oven. Approximately 1-2 g representative sample was taken from each concentrate to determine the recovery of each mineral by using a Frantz isodynamic magnetic separator (Frantz, USA).

Chapter 4. Results and Discussion

The microflotation results of single minerals with IL at a low (50 g/t) and high (500 g/t) dosage are shown in Figure 4.1 and Figure 4.2 respectively. The recovery of mineral generally increases as the collector dosage increases at each pH. The only exception is quartz at pH 3. At this pH, the recovery of quartz decreases significantly from 43% to 12%. From FTIR results (presented later), the species adsorbed on quartz surface are likely $[N_{2222}]^+$, through a weak bonding mechanism. This is in agreement with literature about applying ILs in quartz flotation (Sahoo, et al., 2015; Wang , et al., 2005; Weng, et al., 2013; Sahoo, et al., 2014; Sahoo, et al., 2015). One possible explanation for the decreased recovery as collector concentration increases at pH 3 is a pH-dependent micellization for the $[N_{2222}]$ groups. At low concentration, the $[N_{2222}]^+$ groups are adsorbed onto quartz; their alkyl carbon chains orient toward the water phase, inducing hydrophobicity to the quartz surface. As collector concentration increases, a second layer of the same groups will be attached onto the first layer, possibly by hydrogen bonding between their alkyl chains. Their carbon groups orient towards the first layer, form a micelle structure. The formation of micelle decreases the overall hydrophobicity as the alkyl carbon chains orient toward each other. A similar pH-dependent micellization was also observed for oleate collector (Pope, et al., 1973). However, the micellization is less likely to happen for the [EHEHP] moiety as the micellization is more likely to happen for groups that are less hydrophobic (*i.e.* with shorter carbon chain) (Mrozik , et al., 2008). Due to this reason, for bastnäsite and hematite whose recovery are likely due to the adsorption of phosphonate group (discussed later in sections 4.1.1 and 4.2.1 respectively), the same trend was not observed.

It was also observed that the recovery trends with respect to pH for three minerals are not the same. For instance, the recovery of hematite decreases as pH increases, whereas the recovery of quartz remains constant at about 80% at pH>3 at the same collector dosage (500 g/t). This suggests the recovery mechanism for these minerals might not be the same. Overall, the collectability of IL is higher for quartz and hematite than bastnäsite (shown as higher recovery than bastnäsite at every tested condition). This suggests a reverse flotation route and/or depressants might be required in order to improve the separation efficiency when [N_{2222}][EHEHP] is applied as a collector. Two pH (5 and 7) were chosen for further investigate with the presence of depressants. The reason behind this is that at pH 7, the recovery of bastnäsite is low compared to quartz and hematite, which might mean that it is possible to reverse float quartz and hematite, possibly with a depressant that selectively depresses bastnäsite. At pH 5, the recovery of bastnäsite is the highest among all tested pH, which makes it feasible to explore the possibility to directly float bastnäsite. As introduced previously in the literature review section (section 2.2.4.1.2), sodium silicate, NorligH (a commercial depressant contains calcium lignin sulphonate), and manganese chloride ($MnCl_2$) were chosen to be investigated as depressants.

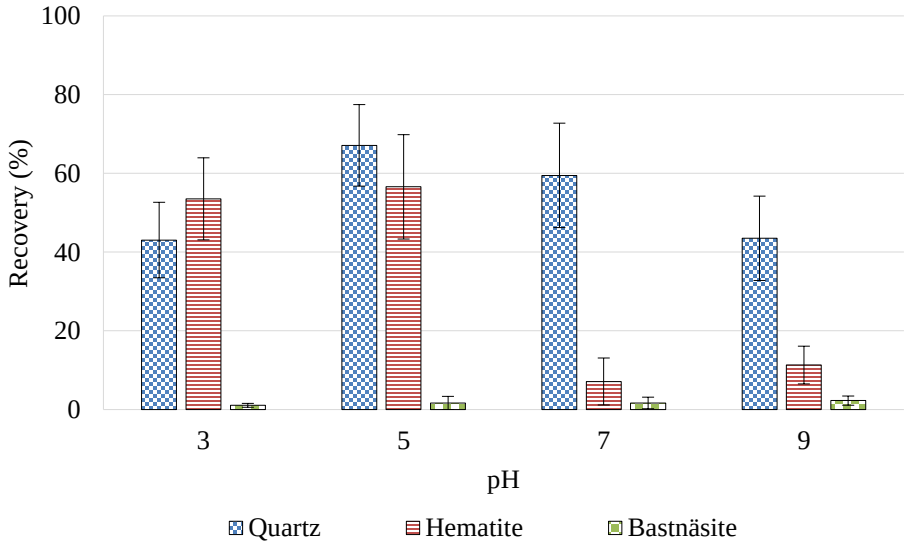

Figure 4.1. Microflotation results with 50 g/t IL as collector, error bars represent 95% confident interval.

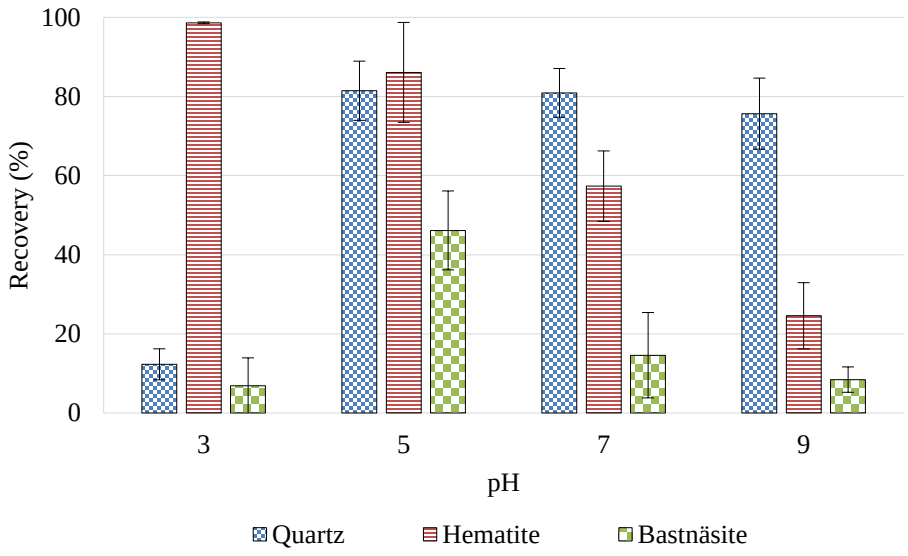

Figure 4.2. Microflotation results with 500 g/t IL as collector.

To study the possibility of increasing the recovery of bastnäsite by increasing the dosage of IL collector, a collector dosage of 1 kg/t was also tested for comparison at pH 5. The results shown in Figure 4.3 indicate that the recovery of bastnäsite increased from 46% to 71%, whereas the increase in recovery for quartz and hematite were much less (13% and 8% respectively). This suggests that the lower collectability for bastnäsite as discussed before might be due to insufficient collector dosage; in comparison, the collecting effect for quartz and hematite is almost saturated at 500 g/t dosage. This result also suggests direct floating bastnäsite might not be feasible in industry since it consumes a large amount of $[N_{2222}][EHEHP]$ to achieve a relative high recovery (71%) for bastnäsite.

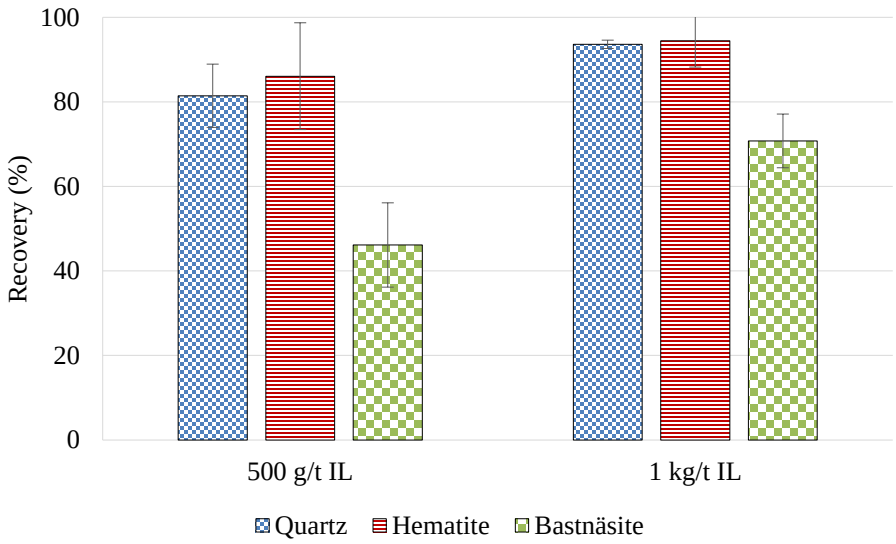

Figure 4.3. Microflotation results with presence of IL at 500 g/t and 1000 g/t dosage at pH 5.

4.1 Bastnäsite

4.1.1 FTIR

The FTIR spectra of pure bastnäsite, IL, and IL-treated bastnäsite at different pH are shown in Figure 4.4. A zoom in look at the 1000-1100 cm^{-1} region is shown on the right. Peaks at 864, 1039, and 1408 cm^{-1} were assigned to CO_3^{2-} vibrations (Azizi, et al., 2016; Sakurai, et al., 1969). Peaks at 2860, 2874, 2929, and 2958 were assigned to C-H stretching vibrations from the alkyl carbon chains (Azizi, et al., 2017; Socrates , 2004). The band near 1037 cm^{-1} in the enlarged figure corresponding to the stretching vibration of asymmetric P–O–C from the phosphonate group (Stuart, 2004). The same band was shifted to 1060 cm^{-1} for bastnäsite treated with IL at pH 3, 5, and 7, which suggest strong chemical bonding between the [EHEHP] moiety and the mineral surface. This is in agreement with previous studies on ILs with similar structures (Azizi, et al., 2016; Sun, et al., 2014). The signal intensity is stronger at pH 5 and 7, which is in agreement with microflotation results that bastnäsite observes the higher recovery at pH 5 (~50%) and pH 7 (~15%) than other pH. The peak at 1085 cm^{-1} for bastnäsite is more obvious at pH 7 and 9, suggesting less uptake of IL at alkaline conditions. This finding is in agreement with (Azizi, et al., 2017) in which the researchers found the recovery for bastnäsite using IL was the highest in mildly acidic (near neutral) pH.

Reagent adsorption can involve formation of precipitates, reagent molecules which interact with metal ions that remove from the mineral surface (Miller, et al., 2007). For this reason, the adsorption is studied along with the ion speciation of the system. As seen in Figure 2.1, Ce^{3+} is the predominant ion when pH is below 7. This metal cation could be naturally attracted by the oppositely charged $[EHEHP]^-$, then chemically bonded and re-deposit onto bastnäsite surface. The metal-phosphonate complex induces hydrophobicity to bastnäsite and results in flotation. As the pH increases, Ce hydroxides include $Ce(OH)^{2+}$, $Ce(OH)_2^+$, and $Ce(OH)_3$ start forming (as shown in Figure 2.1). Although they could also interact with the phosphonate moiety, the interactions are expected to be weaker than Ce^{3+} due to the lower valence numbers. This explanation does not agree with the theory by Aziz et al. (2017) who proposed $RE(OH)_2^+$ and $RE(OH)^{2+}$ are the active centers for chelating formation. At pH 3, the interaction between Ce^{3+} and $[EHEHP]^-$, as well as the interaction between the metal complexes and the mineral surface are expected not as strong as at pH 5. This results in weaker adsorption and therefore lower flotation recovery at pH 3. One analogy to this is the stripping process in hydrometallurgy usually takes place at low pH conditions. One possible explanation for this is that protons could form complexes with REE ions, and therefore hinder the reactions between RE ions and $[EHEHP]^-$ (Sun, et al., 2014).

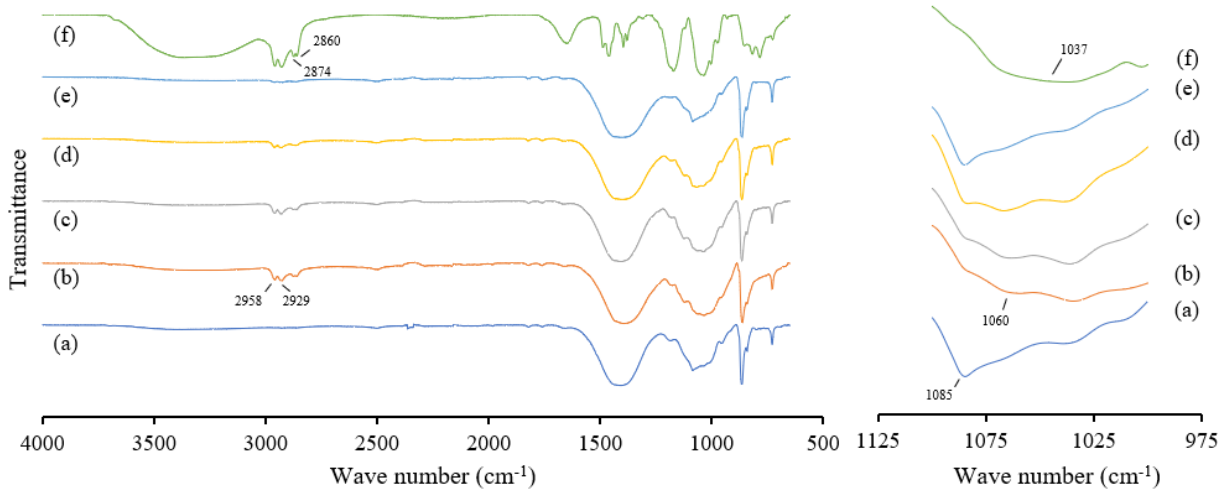

Figure 4.4. FTIR spectra of (a) pure bastnäsite, (b) bastnäsite treated with IL at pH 3, (c) pH 5, (d) pH 7, (e) pH 9, and (f) pure IL.

4.1.2 Zeta potential

Zeta potential of bastnäsite with/without IL and depressants are shown in Figure 4.5. The IEP of bastnäsite was found at 6.8, which is in agreement with literature (Azizi, et al., 2016). The zeta potential of bastnäsite with IL shows an obvious downward shift which indicates the adsorption of the negatively charged phosphonate group. Its adsorption mechanism at pH 7 or higher must be due to chemisorption since the mineral is negatively charged in this range. At pH below 7, the adsorption mechanism cannot be concluded from zeta potential study, since the positively charged mineral particle could naturally attract the anionic phosphonate group.

A more positive shift in zeta potential is observed for bastnäsite with the presence of $MnCl_2$, which might suggest the adsorption of metal cations; in contrast, a downward shift appears for bastnäsite with NorligH, which suggests the adsorption of anionic lignin sulfonate group. Interestingly, zeta potential remains almost unchanged with the presence of sodium silicate, which did significantly depress bastnäsite in microflotation tests (as shown in Figure 4.6). One possible explanation might be that silicate species do not adsorb onto mineral surface directly; they depress the mineral by forming complexes with the metal ions leached from the mineral surface and hinder them from bonding with the collector molecules.

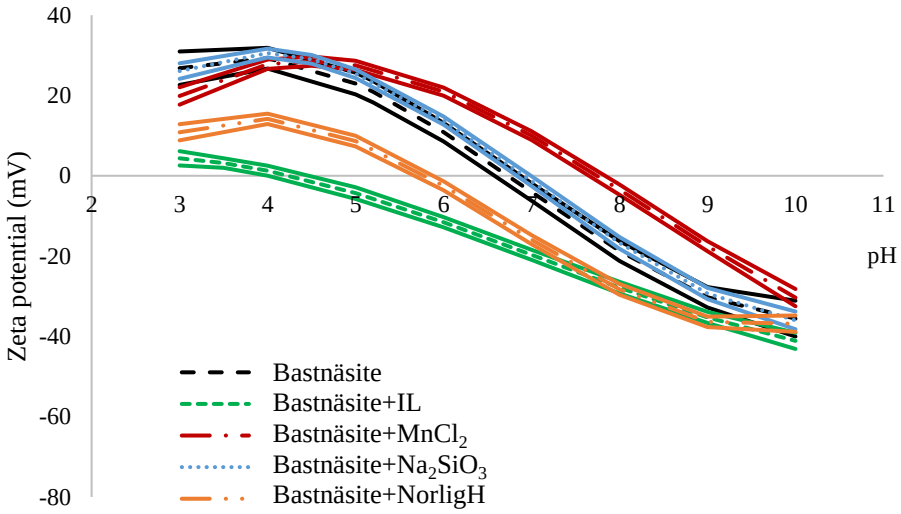

Figure 4.5. Zeta potential of bastnäsite with/without presence of reagent, 95% C.I. calculated by Stata13 statistical software.

4.1.3 Microflotation

The microflotation results of bastnäsite with the presence of depressants are shown in Figure 4.6, in which the results are compared with the cases of IL collector only. The depressing effect of all three depressants was obviously strong that the recovery of bastnäsite decreased to almost zero at all tested conditions. In previous work, researchers applied sodium silicate as depressant for REM flotation; a significant decrease in recovery was also observed, which they explained as incomplete liberation (Azizi, et al., 2016). In this work, the significant depressing effect was observed for pure bastnäsite with the presence of sodium silicate, suggesting the depressing mechanism is more than just incomplete liberation. As shown previously in Figure 2.9, at pH 5 and 7, $Si(OH)_4$ and $SiO(OH)_3^-$ are the dominant ion species, which could be interacting with Ce^{3+} and form new metal complexes. These interactions hinder the interaction between Ce^{3+} and $[EHEHP]^-$, and therefore depress bastnäsite. For $MnCl_2$. Mn^{2+} is the dominant ion specie at pH 5-7 (as shown in Figure 2.10), which might compete with Ce^{3+} in the solution for bonding with $[EHEHP]^-$. Zeta potential measurement also suggest the uptake of positively charged ion species; therefore it is possible that Mn^{2+} is adsorbed and active centers are covered. The depressing effect of lignin sulfonate on bastnäsite has been mentioned in (Krishnamurthy, et al., 2005). The adsorption of lignin sulfonate onto bastnäsite surface was confirmed in an electrokinetic study (Pradip, et al., 2015). In this work, the adsorption and depressing effect of lignin sulfonate for bastnäsite has been confirmed by zeta potential analyses and microflotation tests; possible mechanisms might include depressant molecules cover adsorption centers and block collector adsorption.

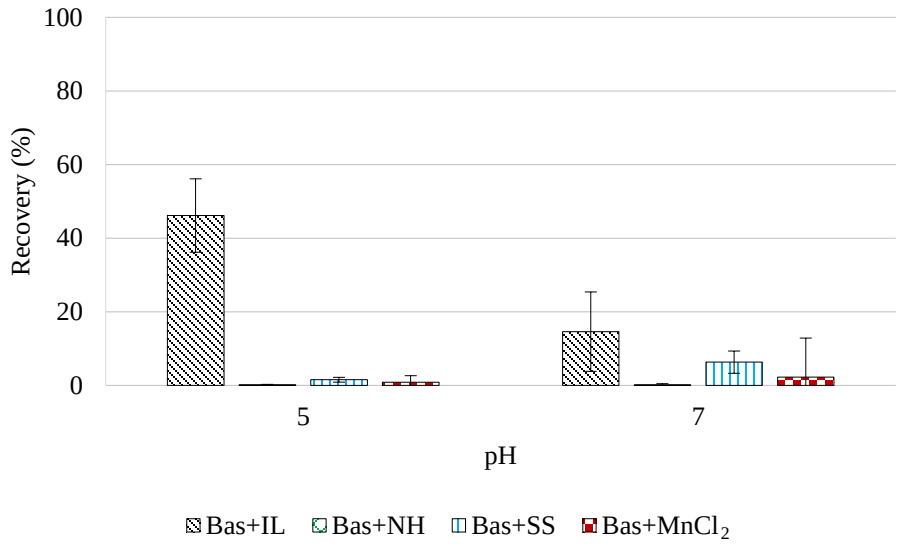

Figure 4.6. Microflotation results of bastnäsite with IL, with/without presence of depressants at pH 5 and 7.

4.2 Hematite

4.2.1 FTIR

The FTIR spectra of pure hematite, IL, as well as IL-treated hematite are shown in Figure 4.7. A closer look at the 2700-3100 cm^{-1} and 1000-1100 cm^{-1} regions are shown at the bottom of the same figure. The same peaks corresponding to C-H stretching vibrations (2860, 2874, 2929, and 2958 cm^{-1}) appear on IL-treated hematite at pH 3 and 5 (weakly), gradually weakened as pH increases. The peaks at 1065 and 1036 cm^{-1} for treated hematite were assigned to P-O-C vibration, which were originally located at around 1037 cm^{-1}. This suggests the phosphonate group is adsorbed onto hematite surface; the shift suggests chemical bonds are involved in the adsorption. The adsorption decreases gradually as pH increases, which correspond well with the trend of microflotation that the recovery of hematite gradually decreases as pH increases.

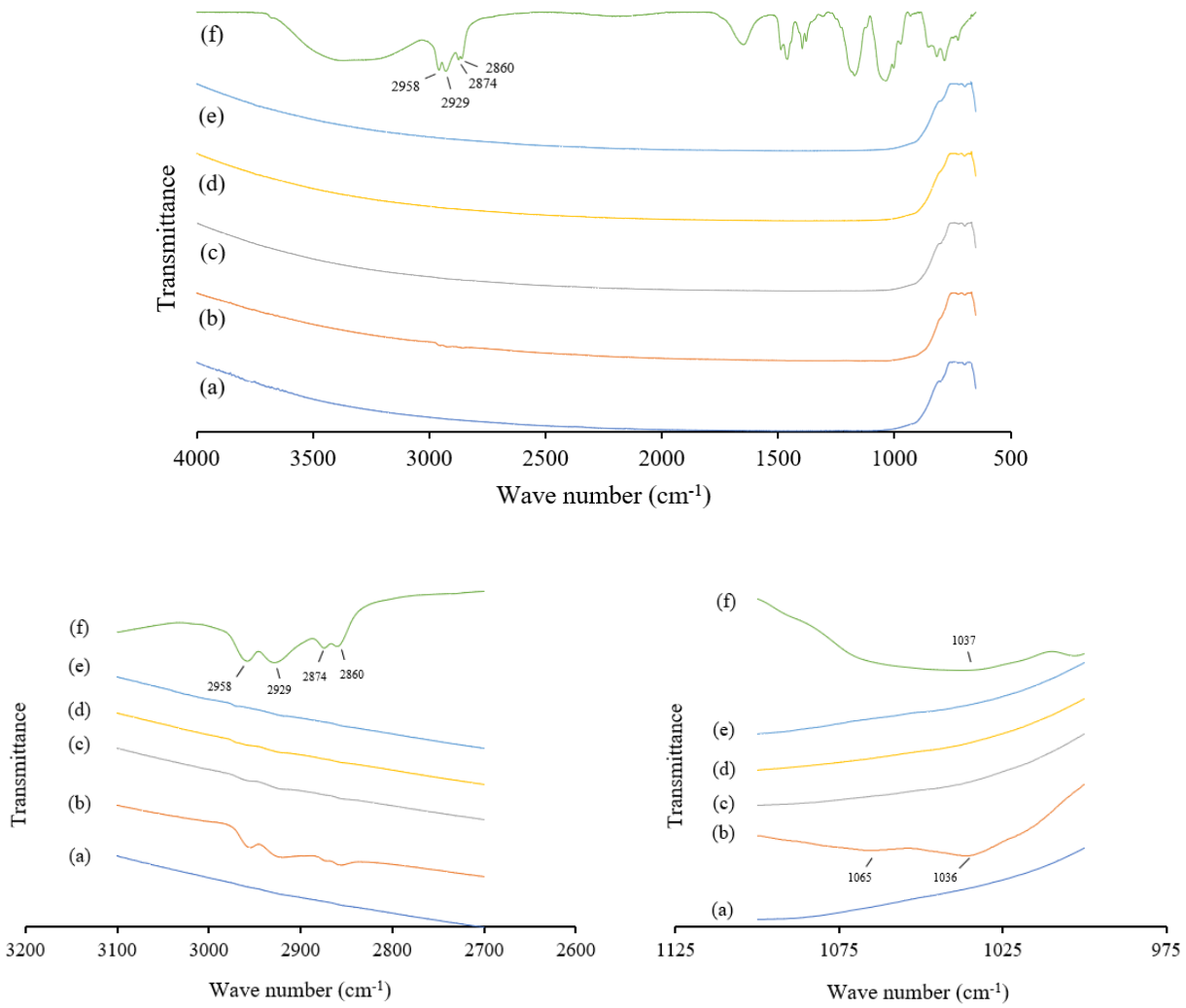

Figure 4.7. FTIR spectra of (a) pure hematite, (b) hematite treated with IL at pH 3, (c) pH 5, (d) pH 7, (e) pH 9, and (f) pure IL.

4.2.2 Zeta potential

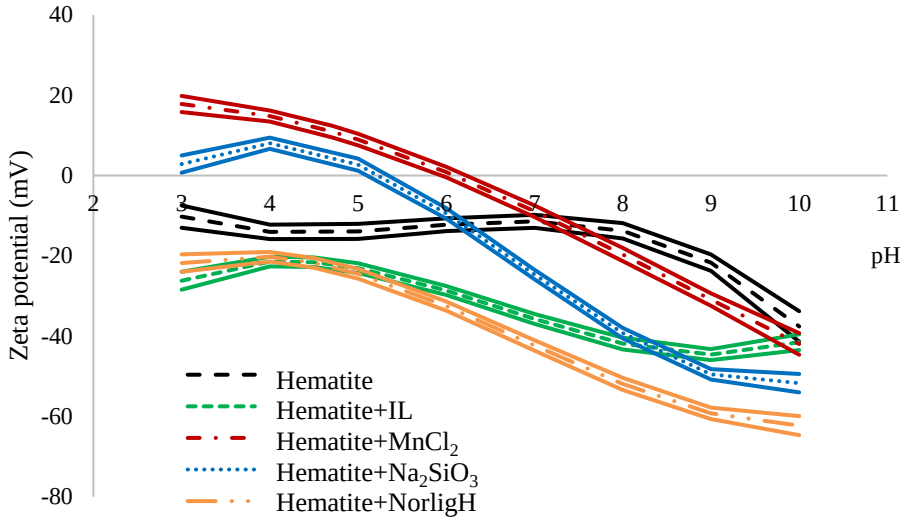

Figure 4.8. Zeta potential of hematite with/without presence of depressant.

Zeta potential of hematite with/without IL and depressants are shown in Figure 4.8. A clear downward shift for hematite with IL suggests the adsorption of anionic $[EHEHP]^-$ onto the hematite surface. The adsorption mechanism is likely chemisorption since the negatively charged hematite surface would naturally repel anionic $[EHEHP]^-$; this is in agreement with the FTIR result, which suggests the formation of chemical bond on hematite after IL treatment. An upward shift in zeta potential is observed with the presence of $MnCl_2$ at pH below 7. In this pH range, the dominant positively charged Mn species are $Mn_2OH^+$and Mn^{2+} as seen in Figure 2.10. They could be adsorbed onto hematite surface and result in positive shift in zeta potential. These metal cations could function in a similar way as for bastnäsite: they could compete with metal cations leached from the mineral surface and bond with $[EHEHP]^-$, and/or cover the adsorption cites on mineral surface to hinder collector adsorption. This therefore results in decreased flotation recovery. As for NorligH, a significant downward shift in zeta potential is observed for hematite. This suggest adsorption of anionic lignin sulfonate group onto mineral surface across the tested pH range. In contrast, sodium silicate results in different trend of shift at different pH: at pH below 6, the zeta potential of hematite observes an upward shift, whereas a downward shift at pH>6. One possible explanation is that at pH below 6, the neutrally charged $Si(OH)_4$ species could adsorb onto hematite and results in a upward shift (closer to zero). At pH>6, negatively charged species such as

$SiO(OH)_3^-$ and $SiO_2(OH)_4^{2-}$ (as shown in Figure 2.9) start to build up on hematite and make zeta potential more negative.

4.2.3 Microflotation

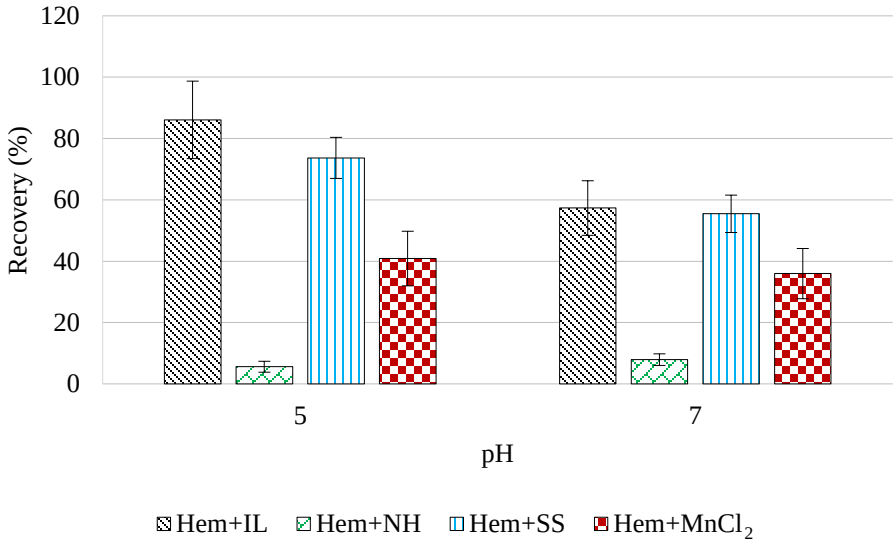

Figure 4.9. Microflotation results of hematite with IL as collector, with/without presence of depressants at pH 5 and 7.

The microflotation results of hematite in the presence of depressants are displayed in Figure 4.9; in the same figure, those results are compared with only IL being present in the system. NorligH shows the highest depressing effect for hematite: at both tested pH, the recovery decreased to negligible values. In contrast, sodium silicate shows only limited depressing effect which is a decrease of approximately 10% at pH 5, and almost no decrease at pH 7. $MnCl_2$ shows a depressing effect for hematite at both pH, the recovery decreased approximately 45% and 20% at pH 5 and 7 respectively.

4.3 Quartz

4.3.1 FTIR

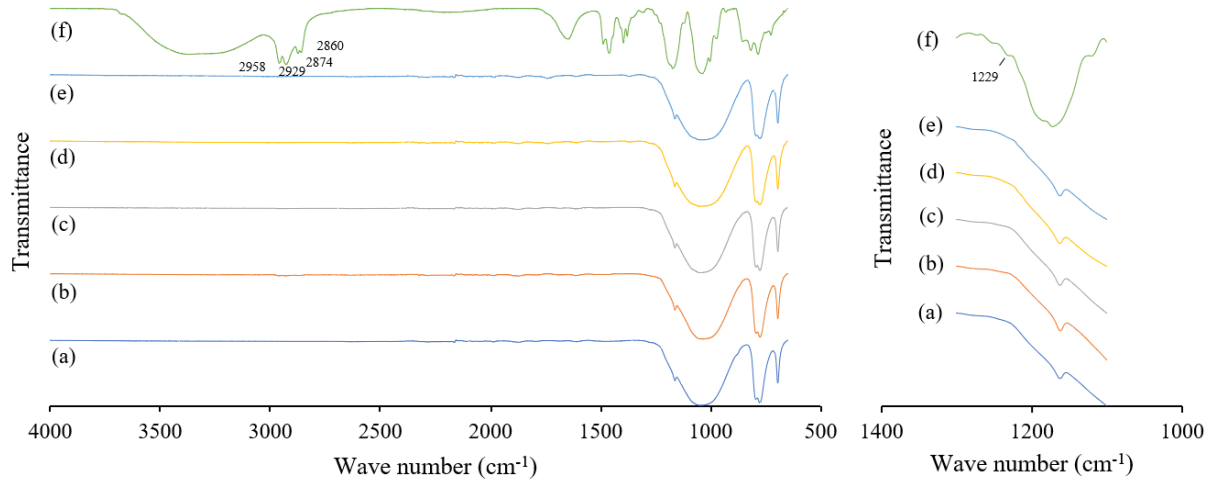

Figure 4.10. FTIR spectra of (a) pure quartz, (b) quartz treated with IL at pH 3, (c) pH 5, (d) pH 7, (e) pH 9, and (f) pure IL.

The FTIR spectra of pure quartz, IL, as well as IL-treated quartz at different pH are shown in Figure 4.10. An enlargement focusing on the 1100-1300 region cm^{-1} is shown on the right. The peak at 1229 cm^{-1} from IL spectrum is assigned to the P=O stretching vibration (Dong, et al., 2015; Wang, et al., 2013; Azizi, et al., 2017). The peak did not show on the treated quartz spectra, which suggests the phosphonate group did not adsorb onto quartz. To explain the high collectability by IL for quartz in microflotation tests, the most likely explanation is the uptake of $[N_{2222}]$ moiety through a weak bonding mechanism; the same groups were washed off when preparing FTIR samples. This could explain the high recovery in flotation with no clear evidence of IL adsorption in the FTIR spectra.

4.3.2 Zeta potential

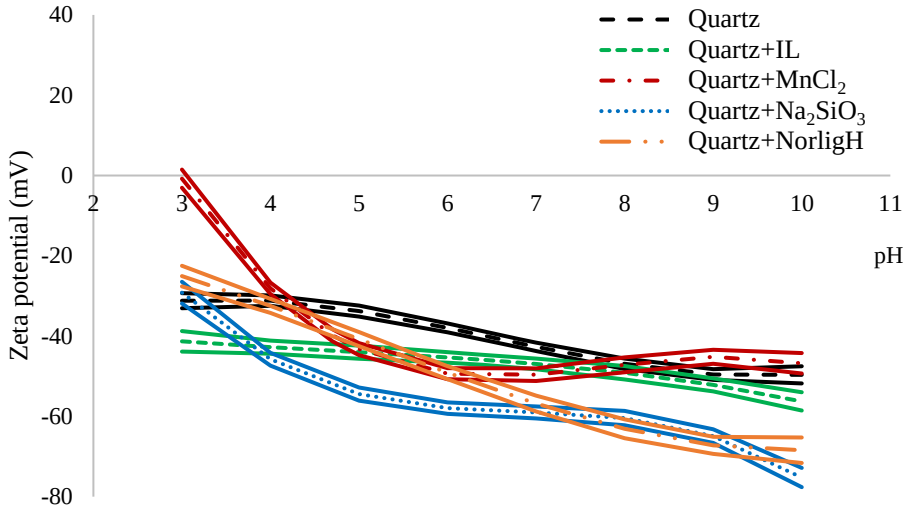

Figure 4.11. Zeta potential of quartz with/without presence of depressant.

Zeta potential of quartz with presence of IL and depressants are shown in Figure 4.11. There is a slight downward shift (maximum about 10 mV) in zeta potential for quartz with IL at pH below 7. Compared to hematite and bastnäsite with IL, this minor shift is not very significant and not conclusive at this point. In addition, from FTIR study, there is no evidence of adsorption of phosphonate group on quartz surface. Possible explanations include dissolution of minor impurities such as Fe resulted in uptake of $[EHEHP]^-$. Further studies are expected to verify the shift in zeta potential for quartz with IL.

For the depressants, the addition of Na_2SiO_3 results in an appreciable downward shift cross the entire pH range. Surprisingly, the negative shift at pH 5 and 7 did not result in significant change in microflotation (as seen in Figure 4.12). This could be due to the superior collecting effect of IL for quartz. In other words, sodium silicate at the tested dosage in microflotation tests might not be sufficient to depress quartz when $[N_{2222}][EHEHP]$ is applied as a collector. To compare, NorligH also shows shift at pH above 4. The difference in the depressing ability between sodium silicate and NorligH could be due to the different structure of Na_2SiO_3 and NorligH: the former has a single molecule form, whereas the latter is an organic compound which has a larger structure. This large structure would cause entanglement near the mineral surface, and therefore prohibit collector from being attached onto the mineral surface. For $MnCl_2$, a slight downward shift (~10 mV) in

zeta potential is observed between pH 4-8, which roughly corresponds to the range where Mn^{2+} is the dominant ion species (as seen in Figure 2.10). In contrast, at pH below 4, a notable positive shift in zeta potential might suggest the deposition of $Mn_2(OH)^+$ onto the quartz surface.

4.3.3 Microflotation

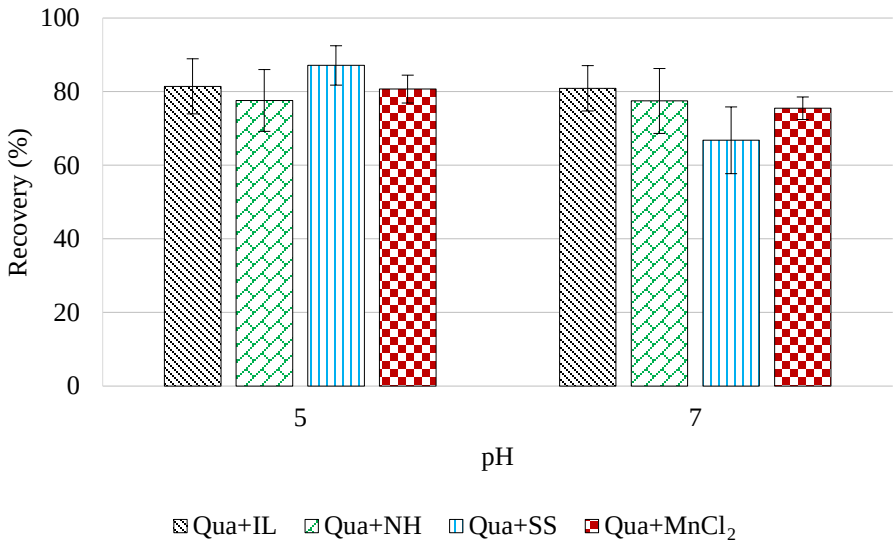

Figure 4.12. Microflotation results of quartz with IL as collector, with/without presence of depressants at pH 5 and 7.

The microflotation results of quartz with the presence of depressants are displayed in Figure 4.12; in the same figure, those results are compared with the cases that only IL is present in the system. Interestingly, sodium silicate does not depress quartz at pH 5, with only approximately 13% decrease on average at pH 7. Even though the decrease at pH 7 is small (*i.e.* the depressing effect of sodium silicate is limited), a Student's t-test confirms that the recovery of quartz in the presence of sodium silicate is statistically different from that with IL only. On another hand, NorligH does not depress quartz at pH 5. Researchers have applied NorligH as a depressant for quartz with amine as collector, and significant depressing effect was observed for quartz (Marion, et al., 2015). Considering their collector and NorligH dosages are similar to this work, the difference in quartz recovery must be due to different collectors applied. This again proves the superior collectability of the tested IL for quartz. For $MnCl_2$, there is almost no depressing effect for quartz when $[N_{2222}][EHEHP]$ is applied as a collector. The limited depressing effect by all three depressants

suggests the superior collectability of IL for quartz, even with the presence of common silicate depressants.

4.4 Bench scale flotation

Due to limitations of the quality of minerals samples available, only preliminary tests (*i.e.* 1 test at each condition) were done for bench flotation at pH 5 with/without the presence of sodium silicate. The dosages of collector and depressant were kept constant at 500 g/t. It can be seen in Figure 4.13 the recovery of hematite and bastnäsite was approximately 65% when only IL is present. It was observed during flotation that both minerals were recovered in an agglomerated form, therefore the high recovery of bastnäsite might be due to interactions with hematite. The recovery of quartz was approximately 55%, which was lower than that for single mineral flotation under the same conditions. When sodium silicate is applied, the recovery of hematite and quartz remained constant, whereas the recovery of bastnäsite showed a significant drop from 65% to 20%. This is in agreement with single mineral microflotation that sodium silicate has little impact on the recovery of quartz and hematite but can significantly depress bastnäsite. These preliminary tests suggest that it is possible to further upgrade bastnäsite from 33% to 52% with 80% recovery using sodium silicate as depressant and IL as collector. In order to achieve better separation results, a higher dosage of IL is expected due to relative low recovery for quartz (~55%); also, a higher dosage of sodium silicate or a more effective bastnäsite depressant is expected since there is still an appreciable amount (~20%) of bastnäsite has been rejected with hematite and quartz. Alternatively, gravity separation might be useful to reject most of quartz prior to flotation in order to achieve a better separation. An example flowsheet is shown in Figure 4.14.

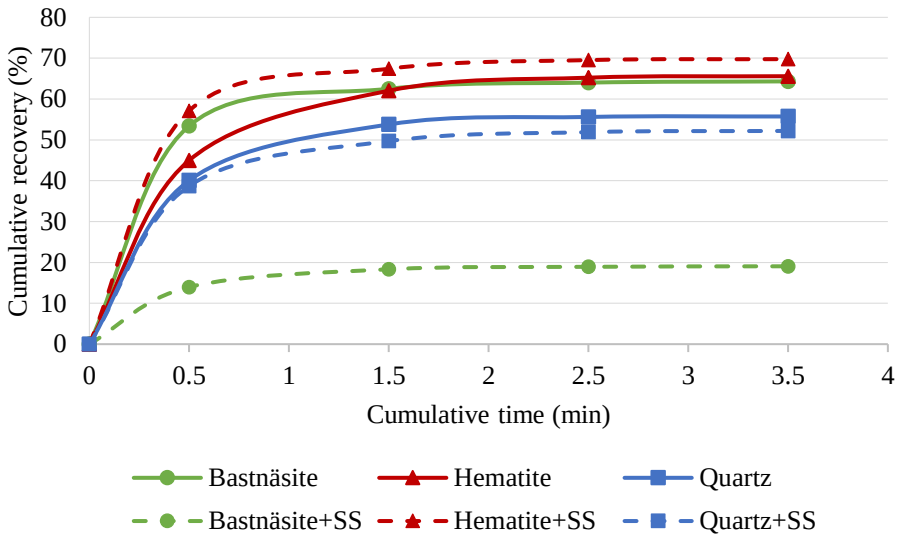

Figure 4.13. Flotation results of the synthetic mixture with/without the presence of sodium silicate at pH 5.

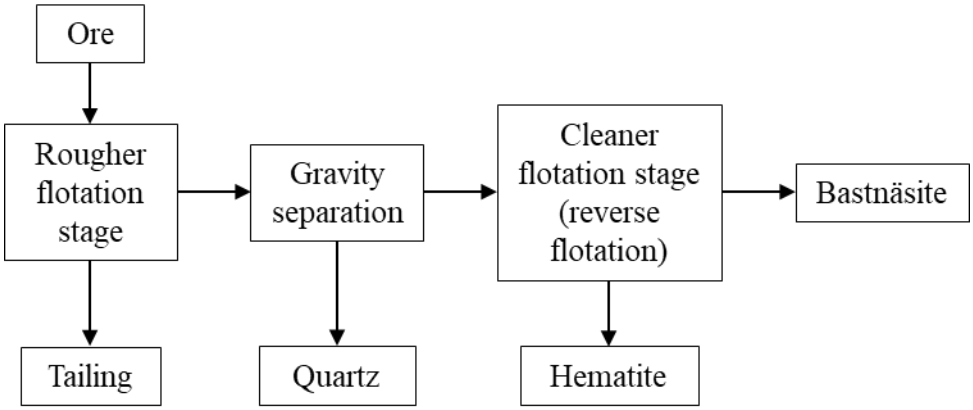

Figure 4.14. A possible flowsheet to separate bastnäsite from hematite and quartz more effectively.

Chapter 5. Conclusions

In this project, one type of IL, $[N_{2222}][EHEHP]$, has been tested for REM flotation for the first time. Bastnäsite was tested as REM, the results of which were compared with quartz and hematite (common gangue minerals). Zeta potential measurements and FTIR studies were applied to investigate the reagent adsorption, which were used to explain minerals' response in microflotation and bench scale flotation. It was found that the [EHEHP] moiety is adsorbed onto hematite and bastnäsite most likely by chemisorption, whereas $[N_{2222}]$ adsorbs onto quartz most likely through weak interaction mechanisms. It was found that the floatability of $[N_{2222}][EHEHP]$ is higher for

quartz and hematite than bastnäsite, shown as higher recovery of quartz and hematite than bastnäsite at all tested conditions. Bastnäsite has its highest recovery (~50%) at pH 5 at 500 g/t [N_{2222}][EHEHP] dosage. Under the same conditions, the recoveries of both quartz and hematite are over 80%, which suggests a reverse flotation route and/or depressants might be required in order to achieve sufficient separation.

Sodium silicate, calcium lignin sulfonate (NorligH), and manganese chloride have been tested as depressants on the model minerals. Interestingly, they have little or limited depressing effect on quartz, suggesting superior collectability of [N_{2222}][EHEHP] for quartz even with the presence of depressants. Hematite is well depressed by NorligH and manganese chloride at specific conditions. All three depressants depressed bastnäsite under all tested conditions, which again suggests a reverse flotation route might be preferable. Based on the single mineral flotation test results, a synthetic mixture of three minerals was tested with the presence of sodium silicate as depressant for bastnäsite at pH 5. Results showed that it was possible to depress bastnäsite selectively at a dosage of 500 g/t sodium silicate, with the recoveries of quartz and hematite remaining high. However, to achieve better separation effect, a higher depressant dosage, or a more effective REM depressant might be tested as future work. In addition, once the optimum flotation condition has been proposed, an actual RE ore will be tested. The concentrates and tail produced from flotation will then be analyzed by characterization techniques including XRD and QEMSCAN.

It is important to notice that in previous work the same IL has been proved with high selectivity towards REEs as solvent extractant. The results obtained in this work show even though it is possible to achieve efficient separation of bastnäsite from quartz and hematite, the amount of reagent and operation costs might potentially make it uneconomical for industrial operations. An optimized flowsheet might be expected as well as a part of future work, based on which an economic analysis could be done.

References

Ansari, A. (2003). The effect of lignosulfonates on the floatability of molybdenite and chalcopyrite.

Arantes, R. S., & Lima, R. M. (2013). Influence of sodium silicate modulus on iron ore flotation with. International Journal of Mineral Processing, 125, 157-160.

Argus Consulting Services. (2015). Argus Rare Earths Monthly Outlook.

Azizi, D., Larachi, F., & Latifi, M. (2016). Ionic-liquid collectors for rare-earth minerals flotation—Case of tetrabutylammonium bis(2-ethylhexyl)-phosphate for monazite andbastnäsite recovery. Colloids and Surfaces A: Physicochemical and Engineering Aspects, 506, 74-86.

Azizi, D., Sarvaramini, A., & Larachi, F. (2017). Liquid-liquid mineral separation via ionic-liquid complexation ofmonazite and bastnäsite—An alternate route for rare-earth mineralbeneficiation. Colloids and Surfaces A: Physicochemical and, 520, 301-323.

Babchin, A. J., Chow, R. S., & Sawatzky, R. P. (1989). Electrokinetic measurements by electroacoustical methods. Advances in Colloid and Interface Science, 30, 111-151.

Berthomieu, C., & Hienerwadel, R. (2009). Fourier transform infrared (FTIR) spectroscopy. Photosynthesis Research, 101, 157-170.

Billinghurst, W. M. (1951). The depression of quartz in sulphide flotation. Missouri University of Science and Technology.

Bogdanov, O. S., Yeropkin, Y. I., Koltunova, T. E., Khobotova, N. P., & Shtchukina, N. E. (1974). Hydroxamic acids as collectors in the flotation of wolframite, cassiterite and pyrochlore. Tenth international mineral processing congress 1973, (pp. 553-564).

Boisen, M. B., & Gibbs, G. V. (1993). A Modeling of the Structure and Compressibility of Quartz with a Molecular Potential and its Transferability to Cristobalite and Coesite. Physics and Chemistry of Minerals, 20, pp. 123-135.

Bulatovic, S. M. (1999). Use of organic polymers in the flotation of polymetallic ores: a review. Minerals Engineering, 12(4), 341-354.

Chen, L. G., Strassburg, S. H., & Bermudez, H. (2016). Micelle co-assembly in surfactant/ionic liquid mixtures. Journal of Colloid and Interface Science, 477, pp. 40-45.

Chen, Z. (2011). Global rare earth resources and scenarios of future rare earth. Journal of Rare Earths, 29(1), 1-6.

Chi, R., Xu, S., Zhu, G., Xu, J., & Qiu, X. (2001). Beneficiation of rare earth ore in china. Technical Sessions at the 130th TMS Annual Meeting (pp. 1159-1165).

Clearfield, A., Reibenspies, J. H., & Bhuvanesh, N. (2008). Principles and Applications of Powder Diffraction.

Colthup, N. B., Daly, L. H., & Wiberley, S. E. (1990). Introduction to Infrared and Raman Spectroscopy (Third Edition).

Cosgrove, T. (2005). Colloid Science Principles, Methods and Applications.

Dong, B., Li, N., Zheng, L., Yu, L., & Inoue, T. (2007). Surface Adsorption and Micelle Formation of Surface Active Ionic Liquids in Aqueous Solution. Langmuir, 23, pp. 4178-4182.

Dong, Y., Sun, X., Wang, Y., & Chai, Y. (2015). The development of an extraction strategy based on EHEHP-type functional ionic liquid for heavy rare earth element separation. Hydrometallurgy, 157, pp. 256-260.

dos Santos, I. D., & Oliveira, J. F. (2007). Utilization of humic acid as a depressant for hematite in the reverse flotation of iron ore. Minerals Engineering, 20, 1003-1007.

Espiritu, E. R., Naseri, S., & Waters, K. E. (2018). Surface chemistry and flotation behavior of dolomite, monazite and bastnäsite in the presence of benzohydroxamate, sodium oleate and phosphoric acid ester collectors. Colloids and Surfaces A, 546, 254-265.

Feng, B., Lu, Y., Feng, Q., & Li, H. (2012). Solution Chemistry of Sodium Silicate and Implications for Pyrite Flotation. Industrial & Engineering Chemistry Research, 51, pp. 12089-12094.

Fernandez, V. (2017). Rare-earth elements market: A historical and financial perspective. Resources Policy, 53, 26-45.

Ferron, C. J., Bulatovic, S. M., & Salter, R. S. (1991). Beneficiation of Rare Earth Oxide Minerals. Materials Science Forum, 70-72, pp. 251-270.

Fornasiero, D., Montalti, M., & Ralston, J. (1995). Kinetics of Adsorption of Ethyl Xanthate on Pyrrhotite In Situ UV and Infrared Spectroscopic Studies. Journal of Colloid and Interface Science, 172, 467-478.

Fuerstenau, D. W., & Pradip. (2005). Zeta potentials in the flotation of oxide and silicate minerals. Advances in Colloid and Interface Science, 114-115, 9-26.

Fuerstenau, D. W., Pradip, Khan, L. A., & Raghavan, S. (1982). An alternate reagent scheme for the flotation of mountain pass rare-earth ore. Proceedings of the 14th International Mineral Processing Congress, pp. 6.1-6.12.

Fuerstenau, M. C., Somasundaran, P., & Fuerstenau, D. W. (1965). Metal Ion Hydrolysis and Surface Charge in Beryl Flotation. pp. 381-391.

Fullam, M., & Grewal, I. (2001). The Knelson Continuous Variable Discharge (CVD) Concentrator.

Geng, F., Liu, J., Zheng, L., Yu, L., Li, Z., Li, G., & Tung, C. (2010). Micelle Formation of Long-Chain Imidazolium Ionic Liquids in Aqueous Solution Measured by Isothermal Titration Microcalorimetry. Journal of Chemical & Engineering Data, 55, pp. 147-151.

Griffiths, P. R., & de Haseth, J. A. (2007). Fourier Transform Infrared Spectrometry.

Gupta, C. K., & Krishnamurthy, N. (1992). In Extractive metallurgy of rare earths, pp. 197-248.

Haerens, K., Matthijs, E., Chmielarz, A., & Van der Bruggen, B. (2009). The use of ionic liquids based on choline chloride for metal deposition: A green alternative? Journal of Environmental Management, 90, 3245-3252.

Hedrick, J. B. (1991). Rare earths. The lanthanides, yttrium, and scandium. Annual report. In Minerals yearbook, 1991 (Vol. 1, pp. 1211-1237).

Higashiyama, Y., & Asano, K. (2007). Recent Progress in Electrostatic Separation Technology. Particulate Science and Technology, 16(1), 77-90.

Intertek. (n.d.). Fourier Transform Infrared Spectroscopy (FTIR) Analysis.

Jin, J., Gao, H., Chen, X., & Peng, Y. (2016). The separation of kyanite from quartz by flotation at acidic pH. Minerals Engineering, pp. 221-228.

Johnson, P. R. (1999). A Comparison of Streaming and Microelectrophoresis Methods for Obtaining the zeta Potential of Granular Porous Media Surfaces. Journal of Colloid and Interface Science, 209, 264-267.

Jordens, A. (2016). The beneficiation of rare earth element-bearing minerals. PhD thesis, McGill University, Mining and Materials Engineering, Montreal.

Jordens, A., Cheng, Y., & Waters, K. E. (2013). A review of the beneficiation of rare earth element bearing minerals. Minerals Engineering, 41, 97-114.

Jordens, A., Marion, C., Kuzmina, O., & Waters, K. E. (2014). Surface chemistry considerations in the flotation of bastnäsite. Minerals Engineering, 66-68, 119-129.

Jordens, A., Marion, C., Langlois, R., Grammatikopoulos, T., Rowson, N. A., & Waters, K. E. (2016). Beneficiation of the Nechalacho rare earth deposit. Part 1: Gravity and magnetic separation. Minerals Engineering, 99, 111-122.

Jordens, A., Marion, C., Langlois, R., Grammatikopoulos, T., Sheridan, R. S., Teng, C., . . . Waters, K. E. (2016). Beneficiation of the Nechalacho rare earth deposit. Part 2: Characterisation of products from gravity and magnetic separation. Minerals Engineering, 99, 96-110.

Jordens, A., Sheridan, R. S., Rowson, N. A., & Waters, K. E. (2014). Processing a rare earth mineral deposit using gravity and magnetic separation. Minerals Engineering, 62, 9-18.

Jungnickel, C., Łuczak, J., Ranke, J., Fernandez, J. F., Muller, A., & Thoming, J. (2008). Micelle formation of imidazolium ionic liquids in aqueous solution. Colloids and Surfaces A: Physicochem. Eng. Aspects, 316, pp. 278-284.

Kaszuba, M., Corbett, J., Watson, F. M., & Jones, A. (2010). High-concentration zeta potential measurements using light-scattering techniques. Philosophical Transactions of the Royal Society, 368, 4439-4451.

Kilbourn, B. T. (1988). Metallurgical Applications of Yttrium and the Lanthanides. Journal of Metals, 40(5), 22-25.

Krishnamurthy, N., & Gupta, C. K. (2005). Extractive Metallurgy of Rare Earths.

Lager, G. A., Jorgensen, J. D., & Rotella, F. J. (1982). Crystal structure and thermal expansion of α−quartz SiO2 at low temperatures. Journal of Applied Physics, 53, pp. 6751-6756.

Larkin, P. (2011). Infrared and Raman Spectroscopy: Principles and Spectral Interpretation.

Lelis, D. F., Leão, V. A., & Lima, R. M. (2016). Effect of EDTA on quartz and hematite flotation with starch/amine in an aqueous solution containing Mn^{2+} ions. REM: International Engineering Journal, 69(4), 479-485.

Li, H., Zhou, Z. A., Xu, Z., & Masliyah, J. H. (2005). Role of Acidified Sodium Silicate in Low Temperature Bitumen Extraction from Poor-Processing Oil Sand Ores. Industrial & Engineering Chemistry Research, 44(13), pp. 4753-4761.

Long, K. R., Van Gosen, B. S., Foley, N. K., & Cordier, D. (2010). The Principal Rare Earth Elements Deposits of the United States—A Summary of Domestic Deposits and a Global Perspective.

Łuczak, J., Jungnickel, C., Joskowska, M., Thöming, J., & Hupka, J. (2009). Thermodynamics of micellization of imidazolium ionic liquids in aqueous solutions. Journal of Colloid and Interface Science, 336, pp. 111-116.

Luo, J., & Chen, X. (1984). Research into the recovery of high-grade rare-earth concentrate from Baotou complex iron ore, China. Processing, Mineral, Metallurgy, Extractive. (pp. 663-675).

Mackenzie, J. M. (1971). Zeta-potential studies in mineral processing. Measurement, techniques, and applications. Minerals Science and Engineering, 3(3), 25-43.

Marion, C., Jordens, A., McCarthy, S., & Grammatikopoulos, T. (2015). An investigation into the flotation of muscovite with an amine collector and calcium lignin sulfonate depressant. Separation and Purification Technology, 149, pp. 216-227.

Miller, J. D., Abdel Khalek, N., Basilio, C., El-Shall, H., Fa, K., Forssberg, K. S., . . . Zhang, P. (2007). Flotation chemistry and technology of nonsulfide minerals. In M. C. Fuerstenau, G. Jameson, & R.-H. Yoon, Froth flotation: a century of innovation (pp. 465-554).

Miller, N. P., & Berg, J. C. (1991). A comparison of electroacoustic and microelectrophoretic zeta potential data for titania in the absence and presence of a poly (vinyl alcohol) adlayer. Colloids and Surfaces, 59, 119-128.

Mrozik, W., Jungnickel, C., Paszkiewicz, M., & Stepnowski, P. (2013). Interaction of Novel Ionic Liquids with Soils. Water Air Soil Pollut, 224(1759), 1-7.

Mrozik, W., Jungnickel, C., Skup, M., & Urbaszek, P. (2008). Determination of the adsorption mechanism of imidazolium type ionic liquids onto kaolinite: implications for their fate and transport in the soil environment. Environmental Chemistry, 5, 299-306.

Nagaraj, D. R., & Ravishankar, S. A. (2007). Flotation reagents-A critical overview from an industry perspective. In M. C. Fuerstenau, G. Jameson, & R.-H. Yoon, Froth flotation: a century of innovation (pp. 375-424).

Park, C.-H., & Jeon, H.-S. (2010). The Effect of Sodium Silicate as pH Modifier and Depressant in the Froth Flotation of Molybdenite Ores. Materials Transactions, 51(7), pp. 1367-1369.

Parks, G. A. (1967). Aqueous Surface Chemistry of Oxides and Complex Oxide Minerals: Isoelectric Point and Zero Point of Charge. In W. Stumm, Equilibrium Concepts in Natural Water Systems (pp. 121-160).

Pope, M. I., & Sutton, D. I. (1973). The Correlation between Froth Flotation Response and Collector Adsorption from Aqueous Solution. Part I. Titanium Dioxide and Ferric Oxide Conditioned in Oleate Sohtions. Powder Technology, 7, 271-279.

Pradip, & Fuerstenau, D. W. (1983). The adsorption of hydroxamate on semi-soluble minerals. Part I: adsorption on barite, calcite and bastnaesite. Colloid and Surface, 8, pp. 103-119.

Pradip, Li, C. C., & Fuerstenau, D. W. (2015). Surface Chemical Characterization of Bastnäsite through Electrokinetics. KONA Powder and Particle Journal, 32, 176-183.

Pugh, R. J. (1989). Macromolecular Organic Depressants in Sulphide Flotation - A Review, 1. Principles, Types and Applications. International Journal of Mineral Processing, 25, 101-130.

Pugh, R. J. (2007). The Physics and Chemistry of Frothers. In M. C. Fuerstenau, G. Jameson, & R.-H. Yoon, Froth flotation: a centure of innovation (pp. 259-282).

Ren, J., Lu, S., Song, S., & Niu, J. (1997). A new collector for rare earth mineral flotation. Minerals Engineering, 10(12), 1395-1404.

Sahoo, H., Rath, S. S., & Das, B. (2014). Use of the ionic liquid-tricaprylmethyl ammonium salicylate (TOMAS) as a flotation collector of quartz. Separation and Purification Technology, 136, 66-73.

Sahoo, H., Rath, S. S., Jena, S. K., Mishra, B. K., & Das, B. (2015). Aliquat-336 as a novel collector for quartz flotation. Advanced Powder Technology, 26, 511-518.

Sahoo, H., Sinha, N., Rath, S. S., & Das, B. (2015). Ionic liquids as novel quartz collectors: Insights from experiments and theory. Chemical Engineering Journal, 273, 46-54.

Sakurai, K.-i., Wakita, H., Kato, A., & Nagashima, K. (1969). Chemical Studies of Minerals Containing Rarer Elements from the Far East. LXIII. Bastnaesite from Karasugawa, Fukushima Prefecture, Japan. Bulletin of the Chemical Society of Japan, 42, 2725-2728.

Silva, J. P., Baltar, C. A., Gonzaga, R. S., Peres, A. E., & Leite, J. Y. (2012). Identification of sodium silicate species used as flotation depressants. Minerals & Metallurgical Processing, 29(4), 207-210.

Socrates, G. (2004). Infrared and Raman Characteristic Group Frequencies: Tables and Charts.

Somasundaran, P., Zhang, L., Healy, T. W., Ducker, W., Herrera-Urbina, R., & Fuerstenau, M. C. (2007). Adsorption of Surfactants and Its Influence on the Hydrodynamics of Flotation. In M. C. Fuerstenau, G. Jameson, & R.-H. Yoon, Froth Flotation: a century of innovation (pp. 179-225).

Spedding, F. H. (1975). Contributions of the rare earths to science and technology. Symposium on the Effects of Rare Earths on the Properties of Metals and Alloys. (pp. 1-11).

Stuart, B. (2004). Infrared Spectroscopy: Fundamentals and Applications.

Sun, X., & Waters, K. E. (2014). Development of Industrial Extractants into Functional Ionic Liquids for Environmentally Friendly Rare Earth Separation. ACS Sustainable Chemistry Engineering, 2(7), 1910-1917.

Sun, X., & Waters, K. E. (2014). Synergistic Effect between Bifunctional Ionic Liquids and a Molecular Extractant for Lanthanide Separation. ACS Sustainable Chemistry Engineering, 2, 2758-2764.

Sun, X., & Waters, K. E. (2014). The Adjustable Synergistic Effects between Acid–Base Coupling Bifunctional Ionic Liquid Extractants for Rare Earth Separation. American Institute of Chemical Engineers, 60(11), 3859-3868.

Sun, X., Ji, Y., Liu, Y., Chen, J., & Li, D. (2010). An Engineering-Purpose Preparation Strategy for Ammonium-Type Ionic Liquid with High Purity. American Institute of Chemical Engineers, 56(4), 989-996.

Thermo Fisher Scientific. (2015). Basic organic functional group reference chart.

Tian, G., Li, J., & Hua, Y. (2010). Application of ionic liquids in hydrometallurgy of nonferrous metals. Transactions of Nonferrous Metals Society of China, 20, 513-520.

U.S. Geological Survey. (2018). Mineral Commodity Summaries 2018: U.S. Geological Survey.

Visser, A. E., Swatloski, R. P., Reichert, W. M., Mayton, R., Sheff, S., Wierzbicki, A., . . . Rogers, R. D. (2002). Task-Specific Ionic Liquids Incorporating Novel Cations for the Coordination and Extraction of Hg^{2+} and Cd^{2+}: Synthesis, Characterization, and Extraction Studies. Environmental Science & Technology, 36(11), 2523-2529.

Wang, Y., & Ren, J. (2005). The flotation of quartz from iron minerals with a combined quaternary ammonium salt. International Journal of Mineral Processing, 77, 116-122.

Wang, C., Qiu, X., Hu, Z., Wang, T., & Li, H. (2014). Flotation Mechanism of Bastnaesite by Salicylhydroxamic Acid. Journal of the Chinese Society of Rare Earths, 32(6), 727-735.

Wang, K., & Liu, Q. (2013). Adsorption of phosphorylated chitosan on mineral surfaces. Colloids and Surfaces A: Physicochemical and Engineering Aspects, 436, 656-663.

Weng, X., Mei, G., Zhao, T., & Zhu, Y. (2013). Utilization of novel ester-containing quaternary ammonium surfactant as cationic collector for iron ore flotation. Separation and Purification Technology, 103, 187-194.

Wills, B. A., & Finch, J. (2016). Wills' Mineral Processing Technology: An Introduction to the Practical Aspects of Ore Treatment and Mineral Recovery.

Yang, F., Kubota, F., Baba, Y., Kamiya, N., & Goto, M. (2013). Selective extraction and recovery of rare earth metals from phosphor powders in waste fluorescent lamps using an ionic liquid system. Journal of Hazardous Materials, 254-255, 79-88.

Zhang, J., & Edwards, C. (2012). A review of rare earth mineral processing technology. 44th Annual Meeting of the Canadian Mineral Processors, CIM, (pp. 79-102).

Zhu, H., Deng, H., & Chen, C. (2015). Flotation separation of andalusite from quartz using sodium petroleum sulfonate as collector. Transactions of Nonferrous Metals Society of China, pp. 1279-1285.

Appendix

A.1 Electrophoretic Zeta potential

As mentioned in previous section for zeta potential, a laser scatter system is used to measure the mobility of charged particles. This system is named as the laser Doppler electrophoresis. It directly measures the small frequency shift Δf in the scatted laser beam that is caused by the movement of a charged particle. A schematic representation of the optical configuration in laser Doppler electrophoresis instrument can be seen in Figure A.1. The correlation between Δf and the particle velocity can be expressed by Eq. (A.1):

$$\Delta f = \frac{2v sin(\theta/2)}{\lambda} \qquad \text{Eq. (A.1)}$$

Where λ is the wave length of laser, and θ is the scattered angle. The velocity is expressed in unit field strength as the electrophoretic mobility U_E, which is converted to zeta potential ζ by Eq. (A.2) (Kaszuba, et al., 2010):

$$U_E = \frac{2\varepsilon\zeta F(\kappa a)}{3\eta} \qquad \text{Eq. (A.2)}$$

Where ε is the dielectric constant of the suspension, η is the viscosity of solution, and κa is the ratio between the radius of curvature of the particle and the double layer thickness (Cosgrove, 2005). $F(\kappa a)$ is named as the Henry function, the value of which is set as 1.5 when the electric double layer of a particle is thin compare to its own radius (known as the Smoluchowski equation) (Kaszuba, et al., 2010). In contrast, when the value of κa is small, the charged particle can be treated as a point charge, and $F(\kappa a)$ is given the value of 1, which is known as the Huckel equation (Cosgrove, 2005).

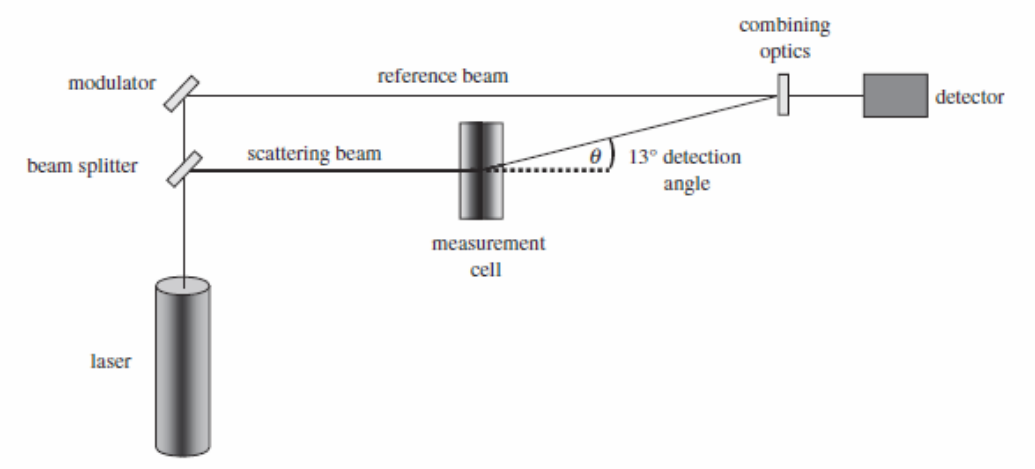

Figure A.1. Schematic presentation of the optical configuration in laser Doppler electrophoresis instrument, adapted from (Kaszuba, et al., 2010).

A.2 FTIR

As mentioned in previous section, FTIR has been applied in the field of mineral processing in order to investigate the bonding species present on top of mineral surface. In the mid-IR region (wavenumber 4000–1000 cm^{-1}), two main types of vibrations exist: stretching vibration, which is along chemical bonds and involves changes in bond length, and bending vibration, which involves changes in the bond angles (Berthomieu, et al., 2009). The stretching vibration can be modeled by harmonic oscillation, in which a chemical bond is represented by a spring linking two points of mass (atoms) (Berthomieu, et al., 2009). The bond strength is represented by k (dyne/cm, 1 dyne=10^{-5} N), and the oscillation frequency ν(cm^{-1}) is given by Eq. (A.3) (Berthomieu, et al., 2009):

$$\nu = \frac{1}{2\pi c}\sqrt{k(m_1 + m_2)/m_1 m_2} \qquad \text{Eq. (A.3)}$$

Where c is the speed of light, m_1 and m_2 are the mass of atoms. From this equation, it can be observed that the frequency of vibration is dependent on the mass of atoms (Berthomieu, et al., 2009). The vibration frequency is also determined by the group environment, electronegativity of neighboring atoms/groups, and hydrogen bonding interaction (Berthomieu, et al., 2009). In a typical IR spectrum, wavenumber is used as horizontal axis, which is directly proportional to the

frequency. Values of wavenumber for some common organic functional groups are shown in Table A.1.

Table A.1. Wavenumbers of IR bands of basic organic functional groups, data adapted from (Thermo Fisher Scientific, 2015).

			$C-H$	$C=C$	$C\equiv C$	Ring	$C-O$	$O-H$	$C=O$	$N-H$	$C\equiv N$
Aliphatic		Methyl	2960	-	-	-	-	-	-	-	-
		Methylene	2930	-	-	-	-	-	-	-	-
Unsaturated	Alkenes	Vinyl	910	1640	-	-	-	-	-	-	
		Vinylidene	890	1640	-	-	-	-	-	-	-
		Cis	700	1640	-	-	-	-	-	-	-
		Trans	965	1670	-	-	-	-	-	-	-
	Alkynes		3200	-	2200	-	-	-	-	-	-
Aromatic		Mono	750	-	-	700	-	-	-	-	-
		Ortho	750	-	-	-	-	-	-	-	-
		Meta	782	-	-	700	-	-	-	-	-
		Para	817	-	-	-	-	-	-	-	-
Oxygen Groups		Ether	-	-	-	-	1100	-	-	-	-
		Alcohol	-	-	-	-	1100	3350	-	-	-
Carbonyl Groups		Aldehyde	2700	-	-	-	-	-	1730	-	-
		Ketone	-	-	-	-	-	-	1700	-	-
		Ester	-	-	-	-	1200	-	1740	-	-
		Carboxylic Acid	-	-	-	-	-	3100	1720	-	-
Nitrogen Groups		Amide	-	-	-	-	-	-	1640	3200	-
		Amine	-	-	-	-	-	-	-	3300	-
		Nitrile	-	-	-	-	-	-	-	-	2250

FTIR also can be coupled with other spectroscopy techniques depends on applications; examples include Diffuse Reflectance Infrared Fourier Transform Spectroscopy (DRIFTS), Thermogravimetric Analysis (FTIR/TGA), Gas Chromatography-Mass Spectrometry (GC/MS), Liquid Chromatography-Mass Spectrometry (LC/MS), UV-Vis, Near IR (NIR) and Raman spectroscopy (Intertek). FTIR combined with these techniques provides complementary information about molecular structure (Intertek).

Many factors could influence IR spectra. For example, sample preparation can be one of them. Figure A.2 shows the IR spectra of sucrose obtained from two different sample preparation routes: prepared as a KBr disc and as a cast film from water (Larkin, 2011). In this example, sample preparation method changes the crystalline and therefore changes the spectra (Larkin, 2011). Sample prepared as a KBr disc results in crystalline solid with many sharp bands; whereas sample prepared as a water cast film becomes amorphous, wider bands with less distinct peaks are observed in the spectrum (Larkin, 2011).

IR spectroscopy is also sensitive to hydrogen bonding (Larkin, 2011). In a simplified molecule model X–H–Y, atom X has high electronegativity and therefore results in ionic X–H bond; whereas H–Y is electrostatic bond with weak covalent characteristics (Larkin, 2011). As a result, hydrogen bonding to the X–H group results in a decreased X–H stretching frequency, shows as a broader and more intense band in the spectrum. Examples include OH and NH groups are strongly influenced by hydrogen bonding (Larkin, 2011). Figure A.3 shows the effect of hydrogen bonding on the O-H stretching frequency. Two compounds are compared in Figure A.3: 2,6-di-tert-butylphenol (with non-hydrogen bonded OH group), and p-creosol (with hydrogen-bonded OH group). It can be observed that the non-hydrogen bonded OH group has a sharp band (at 3645 cm^{-1}) compare to a weaker broader band at 3330 cm^{-1} from the hydrogen bonded OH group (Larkin, 2011).

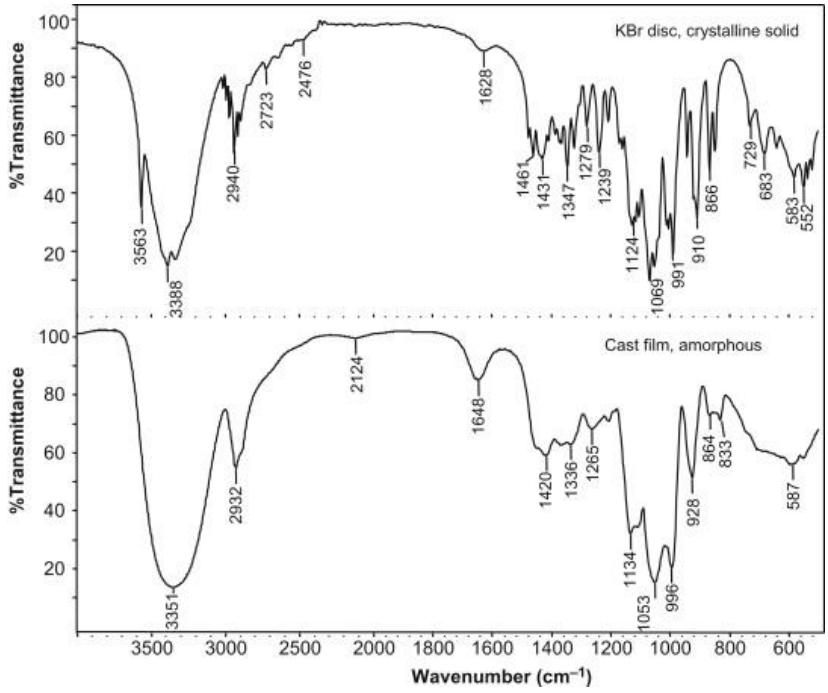

Figure A.2. FTIR spectra of sucrose prepared as a KBr disc (upper) and as a water cast film (lower), adapted from (Larkin, 2011).

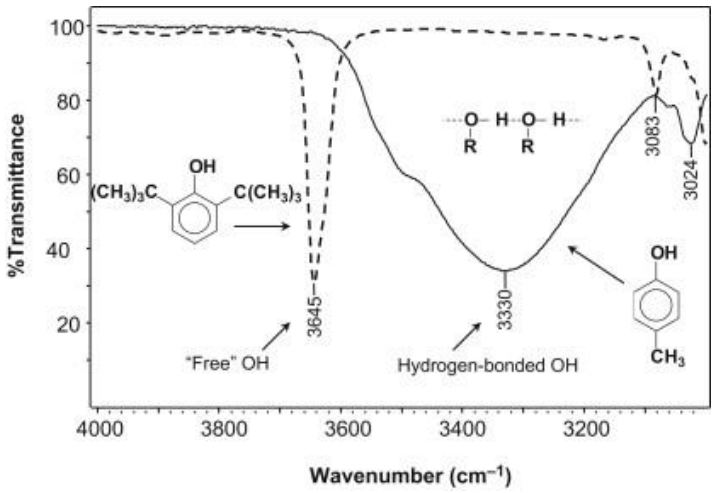

Figure A.3. Solid state FTIR spectra of p-creosol and 2,6-di-tert-butylphenol, adapted from (Larkin, 2011).

It should be noted that, different techniques exist for sample preparation for IR spectroscopy. Generally, the following criteria should be met for appropriate IR sample preparation (Larkin, 2011):

1. The sample should be prepared in a way to achieve uniform thickness and homogeneous composition.
2. The baseline of a spectrum should be relatively flat, and the highest point should be between 95-100% transmittance (or, equivalently, 0-5% absorbance).
3. To compensate the effect of molecules in the atmosphere, the background spectrum should be subtracted.
4. Bands that do not belong to the sample should be eliminated during data analysis.
5. Interested regions of the spectrum can be properly expanded during analysis to reveal detail features.